HIGH-FIELD ASYMMETRIC WAVEFORM ION MOBILITY SPECTROMETRY: EVALUATION OF NOVEL CELL GEOMETRIES AND TECHNIQUES

By

MARILYN PRIETO

A DISSERTATION PRESENTED TO THE GRADUATE SCHOOL
OF THE UNIVERSITY OF FLORIDA IN PARTIAL FULFILLMENT
OF THE REQUIREMENTS FOR THE DEGREE OF
DOCTOR OF PHILOSOPHY

UNIVERSITY OF FLORIDA

2010

To my parents and my beloved husband-to-be, Derick Tourne

ACKNOWLEDGMENTS

The accomplishments of this work are dedicated to those individuals who helped me stay sane during my years at the University of Florida. I would like to extend my deepest gratitude to my advisor, Dr. Richard Yost, for giving me the opportunity to join his research group and for his consistent support and mentoring. His door was always open for anything, whether it was research or personal. He taught me how to be an independent thinker and a successful scientist.

A special thanks goes to all the members of the Yost group for their help, suggestions and friendship. I give special thanks to Leonard Rorrer for always answering the same questions over and over and never seeming to lose his patience. I would like to thank Dr. Jennifer Bryant for all the late nights we spent brooding over the designs and characterizations of the hemispherical cell. I would also like to acknowledge Chia-Wei Tsai for helping me better understand how the square wave performs even when the data do not make sense. I cannot forget to thank Mike Napolitano for reminding me how important it is to stay motivated. I would also like to acknowledge Stacey Ann Benjamin and Julianne McLaughlin who were always there to make me laugh when all I wanted to do was cry. Very special thanks go to the Chemistry Machine Shop members: Todd Prox, Brian Smith and Joe Shalosky for the many hours of fruitful conversations concerning design ideas for all the cells we made. My research would have not progressed as smoothly as it did if it was not for them.

Last, but not least, I would like to thank my family and friends for always believing in me. They have always been my inspiration when I needed it the most. I give special thanks to my mom for making me the woman I am today and always encouraging me to obtain more education. I give special thanks to my dad for teaching me that there is

always something to smile about. My greatest thanks go to one person and one animal. Derick Tourne, you make me the happiest woman in the world and I cannot wait to spend the rest of my life by your side. Kaligula, my beloved cat, may you rest in peace and know that I will never forget all the times you were the only one to receive me at the door. You will always be my most prized possession.

TABLE OF CONTENTS

page

LIST OF TABLES

LIST OF FIGURES

Abstract of Dissertation Presented to the Graduate School
of the University of Florida in Partial Fulfillment of the
Requirements for the Degree of Doctor of Philosophy

A HIGH-FIELD ASYMMETRIC WAVEFORM ION MOBILITY SPECTROMETRY: EVALUATION OF NOVEL CELL GEOMETRIES AND TECHNIQUES

By

Marilyn Prieto

August 2010

Chair: Richard A. Yost
Major: Chemistry

High-field asymmetric ion mobility spectrometry, or FAIMS, is an emerging detection technology that can operate at atmospheric pressure to separate gas-phase ions. Because FAIMS has continuous ion separation capabilities, it is amenable to use in conjunction with a mass spectrometer. This union offers two orthogonal separation methods, one separating ions according to change in their mobility through a gas as a function of field strength and the other according to the ion's mass-to-charge ratio. FAIMS has been utilized to detect peptides, bacteria, chemical warfare agents, and even drugs.

In literature, there is still much to experiment on the role between three-dimensional (3-D) curved cell geometries (spherical, hemispherical, hemi-elliptical, and ovoidal) and two-dimensional (2-D) curved geometries (cylindrical) with ion behavior. Studies encompassing this research focus on exploring the fundamental and practical issues of curved electrode geometries and novel waveform approaches. The marriage of FAIMS and mass spectrometry (MS) was operated with an atmospheric pressure ionization (API) source which was characterized with each particular geometry while

applying it to explosive detection. Results from these experiments provide a greater understanding of the relationship of cell geometry to ion transmission, resolution and resolving power. Although the use of curved surfaces increases sensitivity, resolution is compromised. This effect is more pronounced with increasing curvature and/or surface area. Depending on the application needed by the analyst (more resolution or more transmission), these novel 3D curved electrodes would be valuable to employ.

Subsequent to the optimization of FAIMS parameters with particular geometries, the practicability of a new waveform approach for FAIMS was examined. The high voltage asymmetric waveform typically used consists of overlapping sine waves; here an asymmetric square waveform is used. Comparison of these two waveforms shows that the implementation of a square wave on a miniature planar FAIMS would deliver better separation and resolving power, at some cost in transmission and thus sensitivity.

Finally, once the performance and efficiency of geometry, waveform type, and ionizer was maximized, this novel analytical platform was applied to explosive analysis. Both 3D curved electrodes (hemispherical and spherical) displayed better resolving power and resolution than a commercial cylindrical cell. These novel FAIMS geometries were able to baseline resolve a 2 ppm mixture of five different explosives where the commercial cylindrical cell failed to resolve any.

This research's main goal is to present the first detailed investigation of novel 3-D and 2-D curved geometries while applying two unique waveforms to show its effect on ion behavior in the FAIMS apparatus. Developing and validating the APCI/FAIMS/MS interface allows for better analyte detection with increased resolution, resolving power, and transmission.

CHAPTER 1
INTRODUCTION AND INSTRUMENTATION

Background

More selective, sensitive, and efficient ion separation techniques are paramount for next-generation detection systems. The sensitivity and selectivity of mass spectrometry (MS) over the years, has made it an indispensible tool for modern analytical chemistry. It should be emphasized that mass spectrometry is not a panacea for solving all problems faced by a scientific expert; no single technique is. Nevertheless, it would not be an overstatement to cite MS as a major contributor to the technology that makes it possible for scientists to monitor and enforce environmental, toxicological, and drug regulations.

Despite all the research and development that have been concentrated on ion separation, the demand still exists for techniques with better selectivity and sensitivity and with real-time analysis - especially for explosives. With the potential for increasing domestic terrorist attacks, the detection of hidden explosives has become a subject of major interest. Trace detection of explosives employs a wide variety of analytical methods, including gas chromatography-electron capture detection (GC-ECD)[1], gas chromatography-mass spectrometry (GC-MS)[2-4], liquid chromatography-mass spectrometry (LC-MS)[5, 6], and thin-layer chromatography (TLC).[7]

The methods mentioned above all have limitations. For instance, they are generally either susceptible to thermal degradation (GC-ECD and GC-MS) because of the explosives' low vapor pressure and thermal instability or are too insensitive (LC) because of broader peak shapes and lower peak heights. Furthermore, while ECD is a sensitive means of detecting explosives, it is less selective than the mass

spectrometer.[8] TLC was one of the first techniques used for explosives analysis because of its low cost and its simultaneous analysis of samples;[8] nevertheless, the detection limits of TLC is generally in the low microgram range making it impossible to detect trace quantities.

For the analysis of explosives, mass spectrometry is widely used when coupled with chromatographic separation due to the advantages of high sensitivity, short response time, as well as the additional selectivity available from MS/MS and ion/molecule reactions.[9] However, requirements for sample preparation substantially restrict the capability of mass spectrometry for explosive detection. Different ionization techniques were developed to overcome these limitations, including atmospheric pressure ionization sources such as electrospray ionization (ESI)[5, 6, 10] and atmospheric pressure chemical ionization (APCI).[11, 12]

Thus far, IMS, formerly known as plasma chromatography, has been most widely used for explosives monitoring because of its high sensitivity and amenability to miniaturization for field portable applications.[13] However, a major disadvantage of IMS is the limited selectivity, such that some interferent ions have the same mobility as the analyte ion, and thus can result in a false positive. FAIMS may be able to reduce this problem because it can separate species with identical low-field mobilities.

In recent years, high-field asymmetric waveform ion mobility spectrometry (FAIMS) has been shown to provide high sensitivity, selectivity, and specificity for many analytes when combined with mass spectrometry.[14] Interfacing these techniques allows the use of two orthogonal separation methods, one separating ions based on their differential ion mobility and the other, on their mass-to-charge (*m/*z) ratio. FAIMS is a valuable

separation technique that exhibits low parts per billion (ppb) limits of detection for continuous vapor streams and is suitable as a gas chromatographic detector owing to its fast response and low memory.[15, 16] It also possesses capabilities of separating isomers and providing additional information orthogonal to MS.[17-19] The first FAIMS apparatus was built by Buryakov et al.[20] and consisted of two flat parallel plates for electrodes. Since then, several different geometries have been evaluated and even more have been theoretically proposed, with each geometry having its own specific advantage. For example, a curved cell electrode can provide better sensitivity due to its focusing effect on the ions.[21-23]

FAIMS is an ion mobility technique that operates at atmospheric pressure and room temperature to separate gas-phase ions.[15, 24, 25] Separation of the ions occurs by applying a non-constant high electric field (~10,000 V/cm), that alternates between high and low voltages of opposite polarities. Conventional ion mobility spectrometry (IMS) works on a somewhat similar principle but only uses low electric fields, ~200 V/cm, to drive the ions across the drift tube. Ions in IMS are separated according to their mobility, *K*, in a particular drift gas.[26]

FAIMS and MS are two orthogonal separation methods, which separate ions depending on their differential ion mobility and ratio of *m/z*. Adding a stage of FAIMS separation before mass spectrometry (using an ionization source capable of working under ambient pressure) is beneficial when working with explosives because of its rapid detection, high sensitivity, improved signal-to-noise ratio, and, when curvature is introduced, its ion focusing capabilities.[14, 27]

The waveform design is an essential feature of the overall FAIMS performance, and thus was evaluated in this research. This fundamental investigation shows a promising technique for separating gas-phase ions at atmospheric pressure. Gaining a more comprehensive understanding of how FAIMS geometry, and the applied FAIMS waveforms affect operation, will allow the efficient production of next-generation detection devices.

Introduction to Ion Mobility Spectrometry

Ion mobility spectrometry (IMS), formerly known as plasma chromatography, has been considered a simple and useful, yet relatively low resolution technique, since its inception into the analytical community over thirty years ago. The low resolving power of IMS has made it unattractive to large-scale commercialization, and thus limited its utility in mainstream analytical chemistry. IMS was developed as an analytical technique over 30 years ago.[28-30] Only recently have advances in its technology and design helped analytical chemists realize the full potential of this relatively simple and sensitive method of analysis. During the last decade, IMS has evolved into an inexpensive and powerful technique for the detection of many trace compounds and different compound classes such as chemical warfare agents[31], explosives[32], and drugs of abuse.[33] Recently, IMS has moved into several exciting areas, including high resolution separations, which, when used in tandem with MS,[34] have allowed for interesting investigation into gas-phase conformation of isomeric proteins and peptides[35] as well as fast separation of illicit drugs and their metabolites.[33]

The basic components of an ion mobility spectrometer consist of a sample inlet, ionization source, reaction region, ion gates(s), drift region, and an ion collector or detector. Figure 1-1 illustrates these components in a conventional, unidirectional, gas

flow system employing APCI as the ionization source and a stacked ring drift region design. In traditional IMS, the sample is introduced into the reaction region with an inert carrier gas. The ions formed are directed toward the drift region by an applied electric field (1-500 V/cm) upon the drift rings. A narrow pulse of ions is injected into the drift region, using an ion gate. Ions travel through a buffer gas at atmospheric pressure, and collisions with the buffer gas help slow the ions down as they travel through the drift tube. In the drift region, the ions are separated based upon their charge and size. The analytical signal is obtained when the ions reach the detector.

The larger the collisional cross section of the ion, the more collisions it experiences and thus the more time it requires to reach the detector. Thus, higher mobilities will be obtained by smaller ions, as shown in equations 1-1 to 1-4. Equation 1-1 demonstrates that the velocity (v_d , cm s^{-1}) of an ion is equal to its mobility (K, cm^2 V^{-1} s^{-1}) times the electric field (E, V/cm). An ion's mobility can be calculated using the length of the drift tube (d, cm) and the drift time (t_d, s), as shown in equation 1-2.

$$v_d = KE = \frac{d}{t_d} \quad (1\text{-}1)$$

$$K = \frac{d}{t_d\, E} \quad (1\text{-}2)$$

The ion's reduced mobility (K_0) is calculated by correcting for standard temperature (T, in Kelvin) and pressure (P, in Torr) conditions, as shown in equation 1-3.

$$K_0 = \frac{273\ P}{(760\ T)} K \quad (1\text{-}3)$$

At low electric fields, the relationship between the ion mobility and experimental conditions is described by equation 1-4, where q is the ion's charge (, N is the number

density of the drift gas, μ is the ion's reduced mass, k is the Boltzmann constant, T is the drift gas temperature in Kelvin, and Ω_D is the collisional cross section.[36, 37]

$$K = \left(\frac{3q}{16N}\right)\left(\frac{2\pi}{\mu kT}\right)^{\frac{1}{2}}\frac{1}{\Omega_D} \quad (1\text{-}4)$$

For IMS, as for any separation technique, the ability to resolve closely spaced peaks is of considerable interest. Resolving power, $R_{p\,IMS}$, as shown in equation 1-5, measures the ability of such an instrument to distinguish two tightly spaced peaks in a single broad peak by dividing the drift time of the peak (t_d) by its width at half height ($W_{\frac{1}{2}}$). Although high resolution IMS has been reported in which resolving powers exceeded some chromatographic systems,[38] resolving powers no greater than 30 have been reported[39] for most commercial instruments. Sensitivity levels of an IMS instrument can be enhanced by increasing the electric field strength of the drift tube or by altering the composition of the drift gas[32, 34].

$$R_{p\,IMS} = \frac{t_d}{W_{\frac{1}{2}}} \quad (1\text{-}5)$$

Introduction to High-Field Asymmetric Waveform Ion Mobility Spectrometry

High-field asymmetric waveform ion mobility spectrometry (FAIMS) is a relatively new technique that separates gas-phase ions at atmospheric pressure and room temperature.[14] FAIMS works similarly to IMS, in which the motion of ions is moved along the drift tube with an electric field at atmospheric pressure. However, FAIMS utilizes a non-homogeneous high electric field (>10,000 V/cm) to separate the ions, whereas IMS uses a homogeneous voltage gradient in the 500 V/cm range.

Ions in IMS are separated according to their mobility, K, in a particular drift gas, and their mobility is independent of the applied field; ions will move through the drift

tube at a velocity given equation 1-1. At the higher electric fields employed in FAIMS, K becomes dependent on the applied field, and is better described as the ion's high-field mobility, or K_h.[40] The dependence of an ion's mobility on field strength allows FAIMS its separation power. Specifically, ions are separated in FAIMS by their difference in mobility at high (K_h) and low (K) electric fields. At a constant gas number density, N, the non-linear dependence of the ion's mobility in high electric fields is given by

$$K_h(E) = K\left[1 + \alpha\left(\frac{E}{N}\right)^2 + \beta\left(\frac{E}{N}\right)^4 + \ldots\right] \quad (1\text{-}6)$$

where K is the ion mobility coefficient at low electric fields and α and β are coefficients found experimentally that describe the dependence of the ion's mobility at a high electric field in a particular drift gas.[40] Equation 1-6 is an infinite polynomial series, but at realistic field intensities the terms above the fourth order become insignificant.[41, 42] Equation 1-6 provides a method to describe the change in mobility of an ion in a strong electric field, and to ascertain the mobility of that ion as a function of the strength of the electric field.

In FAIMS, one of the electrodes is typically held at a ground potential while the other has an asymmetric waveform applied to it. The asymmetric waveform, described by $V(t)$, consists of a high voltage component (V_1), labeled in this dissertation as the dispersion voltage (DV), which lasts for a short period of time relative to a longer lasting low voltage component (V_2) of opposite polarity. The waveform is constructed so that the voltage-time product applied to the electrode is equal to zero, as shown in equation 1-7.

$$V_1 t_1 + V_2 t_2 = 0 \quad (1\text{-}7)$$

At high electric fields, the application of this waveform will cause an ion to experience a net drift toward one of the plates as illustrated in figure 1-2. Ions passing between the electrodes encounter this net displacement from their original position because the ion's mobility during the high-voltage component is different than that from the low-voltage mobility.[40] In other words, some ions will move farther during the high-voltage portion than during the low-voltage portion, whereas others will move a shorter distance. These ions will continue to migrate towards one of the plates and subsequently be lost unless a constant direct-current compensation voltage (CV) is applied to offset the drift. The CV required to offset the drift of different ions will be different if the K_h/K ratio of the ions are different. Thus, a mixture of compounds can be successfully separated by scanning the CV, and allowing each ion to transmit at their particular CV, creating a CV spectrum.

When higher electric fields are applied to ions in FAIMS, the ion can have three possible changes in ion mobility as illustrated in figure 1-3. At high-electric fields, the mobility of type A ions increases with increasing electric field strength, whereas the mobility of type C ions decreases, and the mobility of type B ions initially increases before decreasing at yet higher fields.[14] Different polarity waveforms can be used with either positive (P) or negative (N) ions. In curved geometry, the FAIMS instrument is operated in four modes; P1, P2, N1, and N2. The P and N describe the ion polarity and the '1' and '2' indicate the waveform polarity. The waveform with positive DV yields spectra of types P1 and N2, whereas the reversed polarity yields P2 and N1 type spectra.[43]

The ability to explore how geometry affects the performance of FAIMS is essential to thoroughly understanding its capabilities. It has been shown that in a flat plate design, the ions are evenly distributed within the entire analyzer region between the plates, and are continuously being lost to diffusion and space charge repulsion.[22] When curvature is introduced into the geometry of the cell, the ions are focused towards a fixed radial distance.[22] This generally improves transmission but limits resolving power. With a curved geometry, there is still diffusion and space charge effects, but the ions remain distributed within the focused region. Note that ion focusing in curved geometries only occurs in the direction of the applied electric field and thus, lateral diffusion still takes place.

FAIMS offers many advantages as an ion separation tool,[44] since it is able to separate gas-phase ions at atmospheric pressure and temperature, provides high sensitivity with curved cell geometry, it separates and processes ions continuously, and it interfaces easily to a mass spectrometer.

Quadrupole Ion Trap Mass Spectrometry

The quadrupole ion trap mass spectrometer (QITMS) has been widely adopted for chemical analysis because of its selectivity, low detection limits, and broad applicability.[45] Briefly, an ion trap is any device that is capable of trapping and storing ions in a confined space for a period of time. The operation of a quadrupole ion trap (QIT) was initially described by Paul and Steinwedel in a patent filed in 1953 in Germany and awarded as a U.S. patent in 1960.[46] The QITMS traps ions in a controlled manner and is similar to a quadrupole mass filter because it uses oscillating electric fields. However, in the QIT, the ions are trapped in a three-dimensional space, whereas the quadrupole mass filter only confines the ions into two-dimensions.[47]

Quadrupole Ion Trap Theory

The QIT allows for the confinement of ions in a small volume with a three-electrode device consisting of a ring electrode placed between two endcap electrodes (figure 1-4). The endcap electrodes are held at ground potential while radio frequency (RF) (and sometimes direct current (DC)) potentials are applied to the ring electrode. A quadrupolar field is created that can trap ions. The RF potential induces oscillations of the ions to hold the ions within the QIT and is characterized by its amplitude (0 to 8500 $V_{0\text{-}p}$) and its frequency (typically 760 kHz). A potential well difference is created within in the trap by applying a DC voltage (U) and an AC voltage (V), at a particular frequency. This potential difference produces a dynamic electric field for the trapping of ions.

Ions stored in the trap follow trajectories described by the Mathieu equation. Solutions to the second-order differential Mathieu equation are in terms of two reduced parameters, a_z and q_z, which are defined in equations 1-8 and 1-9. These parameters will determine whether or not the ion will possess a stable trajectory inside the trap.

$$a_z = -2a_r = -\frac{16eU}{m(r_0^2 + 2z_0^2)\Omega^2} \quad (1\text{-}8)$$

$$q_z = -2q_r = \frac{8eV}{m(r_0^2 + 2z_0^2)\Omega^2} \quad (1\text{-}9)$$

where the subscripts z and r represent axial and radial motion between and perpendicular to the endcaps, respectively; U is the amplitude of the DC voltage applied to the ring electrode, V is the RF potential applied to the ring electrode, e is the charge on an electron (1.602 x 10^{-19} C), m is the mass of the ion, Ω is the drive frequency ($2\pi f$, where f is the drive frequency in s^{-1}), and r_0 and z_0 are the trap dimensions, as defined

in figure 1-4. From this equation, on can note that q_r is directly proportional to the RF amplitude on the ring electrode, and a_r is proportional to the DC voltage applied.

An ion that is trapped follows a stable trajectory that has the general appearance of a Lissajous motion as shown in figure 1-5. An ion that is unstable will have a trajectory that increases in magnitude towards the endcaps or the ring, and thus will be lost through collisions with the electrodes. In order for an ion to be effectively trapped, its trajectory must be stable in both directions. The solution parameters, a_z and q_z, can be mapped to generate the Mathieu stability diagram (figure 1-6). This diagram describes the common region in (a_z, q_z) space where both the axial and radial components of the ions trajectory are simultaneously stable. This region of stability is defined by the boundaries at $\beta_z = 0$, $\beta_z = 1$, $\beta_r = 0$, and $\beta_r = 1$. An ion that possesses an a_z and q_z value confined by these values will be stable in both the r and z directions, and will be available for mass analysis.

Finnigan LCQ – A Commercial QITMS

All experiments reported in this research were performed on a commercial benchtop Thermo LCQ QITMS. This instrument is equipped with two external atmospheric pressure ionization (API) sources: atmospheric pressure chemical ionization (APCI), and electrospray ionization (ESI). The system is easily operated in both positive and negative ion mode.

For APCI, the sample solution in this research is infused by a syringe pump at a flow rate of 15 µL/min, and vaporized by the standard LCQ APCI heated nebulizer. Once ions are formed, the fully or partially desolvated ions are sampled by a heated capillary, as shown in figure 1-7. The ions then pass through a tube lens and skimmer

cone and into a series of octapole ion guides before making it into the ion trap. Figure 1-7 shows a schematic of the Finnigan LCQ ion trap mass spectrometer.

The exit of the heated capillary, the tube lens, and the skimmer are held under vacuum (1 Torr). The capillary is heated to help in the desolvation process. Ions are then gated through the skimmer cone using the tube lens. A mass-dependent potential is applied to the tube lens so the ions are focused towards the inlet of the skimmer. The skimmer also acts as a vacuum baffle between the skimmer region (1 Torr) and the first octapole region (10^{-3} Torr). The ions are then collected by the first octapole and transmitted to the second octapole through an interoctapole lens. The interoctapole lens assists in focusing of the ions as well as serving as a baffle between the first octapole region (10^{-3} Torr) and the analyzer region ($2x10^{-5}$ Torr).

The ion optics guide ions into the QIT mass analyzer where mass analysis occurs (figure 1-4). In order to inject ions into the trap, an offset voltage of +10V for negative ions and -10V for positive ions is applied to the mass analyzer electrodes. The LCQ QIT operates along the $a_z = 0$ line in the Mathieu stability diagram (figure 1-6) i.e., the DC potential difference between the ring electrode and the endcap electrodes is zero.)

The LCQ QIT utilizes resonant ejection, or axial modulation, to eject ions from the ion trap. Mass analysis is accomplished by ramping the RF voltage on the ring electrode, such that ions of increasing *m/z* consecutively come into resonance with the axial modulation waveform. The ions gain kinetic energy and are ejected in the z direction. The ion detection system includes a 15-kV conversion dynode and a channel electron multiplier.

Atmospheric Pressure Chemical Ionization (APCI)

Gas-phase ions in this research are produced with an APCI source illustrated in figure 1-8. APCI is a gas-phase ionization technique that allows the transfer of ions to the gas phase through ion-molecule reactions at atmospheric pressure. The ionizing reactions of APCI are similar to those of classic CI, although CI is operated under vacuum (~1 Torr). Low-energy electrons are emitted from a corona discharge and initiate the ionization in the source. Analytes in solution are introduced with a syringe pump, are nebulized by a high-speed nitrogen sheath gas flow, pass through a temperature-controlled heater to be vaporized, and are finally ionized by the corona discharge needle. The corona discharge initiates chemical ionization at atmospheric pressure using nitrogen and vaporized solvent as the reagent gas. APCI provides high ionization efficiency since the mean free path of ions at 760 Torr is very short and the number of collisions between reagent ions and analyte molecules is consequently very high.

In APCI, the degree of fragmentation is generally quite low, determined by the amount of energy transferred in the ion-molecule reactions. These ion-molecule reactions include proton transfer, charge exchange, electrophilic or nucleophilic addition, and anion abstraction or nucleophilic displacement. For negative ions, proton transfer takes place when a reagent ion (X^-) accepts a proton from an analyte molecule (MH), as illustrated in equation 1-10. Since H_2O has the highest proton affinity of those gases normally present at ambient conditions, it captures any free protons and, upon collisions with other molecules of H_2O, forms a series of protonated water clusters.[47]

$$X^- + MH \rightarrow XH + M^- \qquad (1\text{-}10)$$

An alternative ionization method to proton transfer is charge exchange. This method typically occurs when the analyte molecule does not contain any acidic or basic sites. Charge exchange occurs in the negative mode when the reactant ion (usually O_2^-) has a recombination energy higher than the ionizing energy of the sample. Additionally, with negative ions, stable complexes may be formed by nucleophilic attack (equation 1-11) with reagent ions of low proton affinity, such as Cl^- and O_2^-. Finally, anion abstraction can also occur with negative ions (equation 1-12). These reactions occur when reagent ions react with sample molecules, resulting in fragment ions from the sample.

$$M + X^- \rightarrow MX^- \quad (1\text{-}11)$$

$$AB + X^- \rightarrow BX + A^- \quad (1\text{-}12)$$

Overview of Dissertation

This dissertation is organized into four chapters. Chapter 1 is an introduction to the research and gives background information on ion mobility spectrometry (IMS) and high-field asymmetric waveform ion mobility spectrometry (FAIMS). Chapter 1 also briefly discusses the instrumentation that was utilized in this research, including ion trap mass spectrometry and atmospheric pressure chemical ionization (APCI).

Chapter 2 explores the fundamental and practical issues of curved electrode geometries in FAIMS. Explicit geometries explored include 3-D curved geometries (spherical and hemispherical) with comparisons to a 2-D curved geometry (cylindrical). Results from these experiments help provide a greater understanding of the relationship of cell geometry to ion transmission and resolution.

In Chapter 3, a novel FAIMS waveform approach is evaluated. The advantages and disadvantages of the application of the asymmetric square waveforms compared to

the traditional sum-of-sine waveform will be discussed. Effects of waveform frequency, duty cycle, and voltage pulse amplitude are also discussed.

Chapter 4 summarizes the major conclusions presented in this work and gives suggestions for future work in this area. The advantages and disadvantages of curved geometries and different waveform approaches for FAIMS are evaluated.

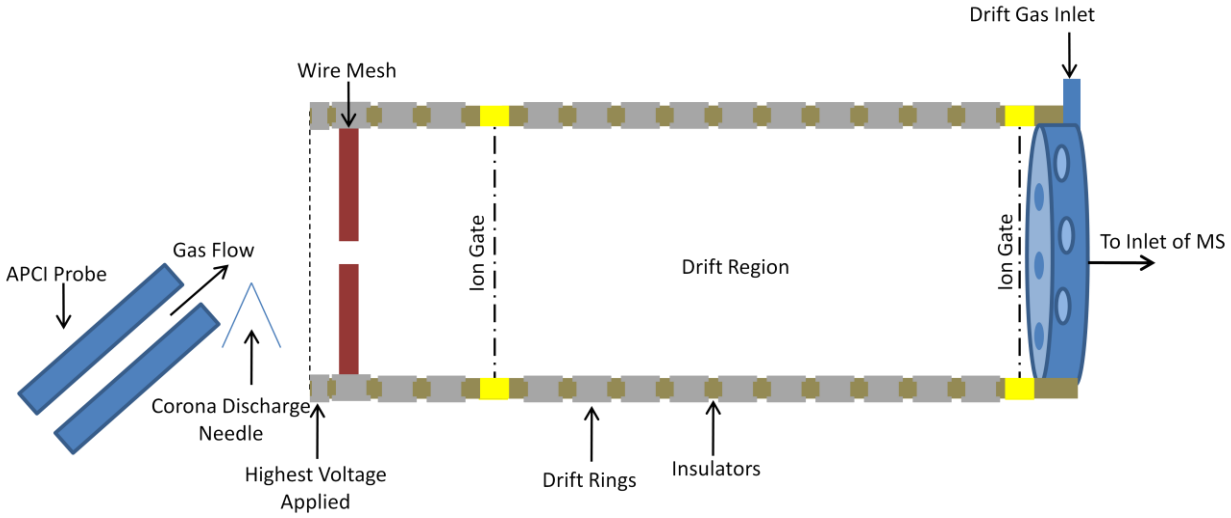

Figure 1-1. Schematic of a characteristic ion mobility spectrometer using the stacked ring design.

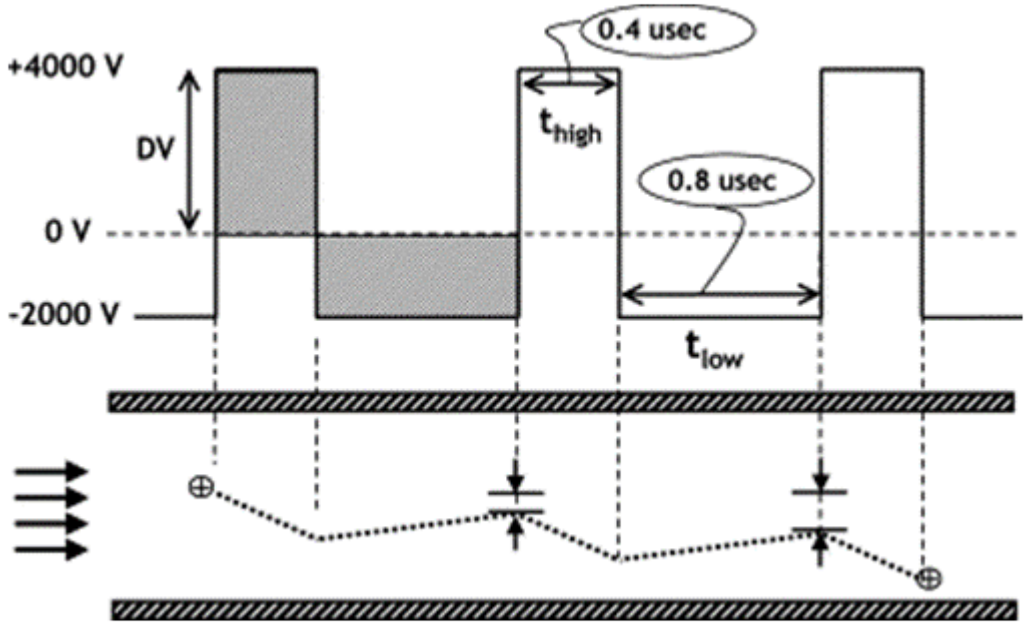

Figure 1-2. Ion motion between two plates during the application of an electric potential. A simplified asymmetric waveform is applied to the upper plate.[40]

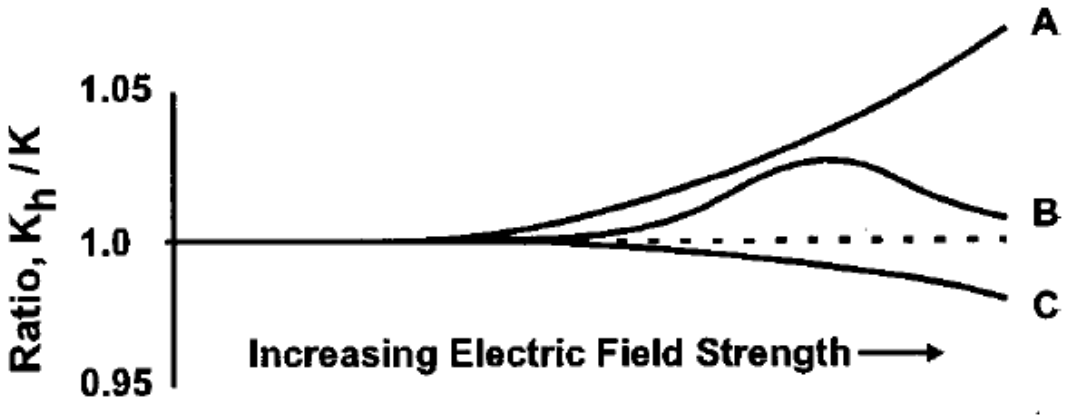

Figure 1-3. Hypothetical plots of the dependence of ion mobility on electric field strength for three types of ions.[14]

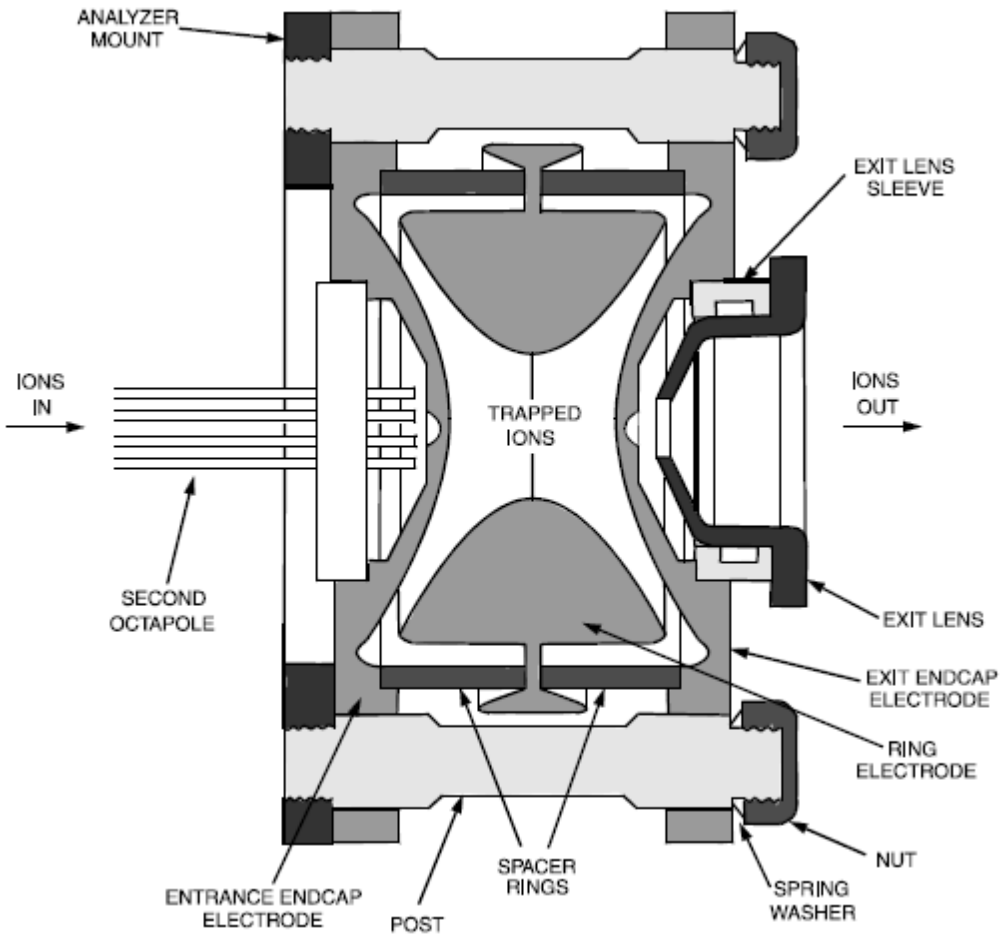

Figure 1-4. Cross sectional view of mass analyzer in the QITMS.[48]

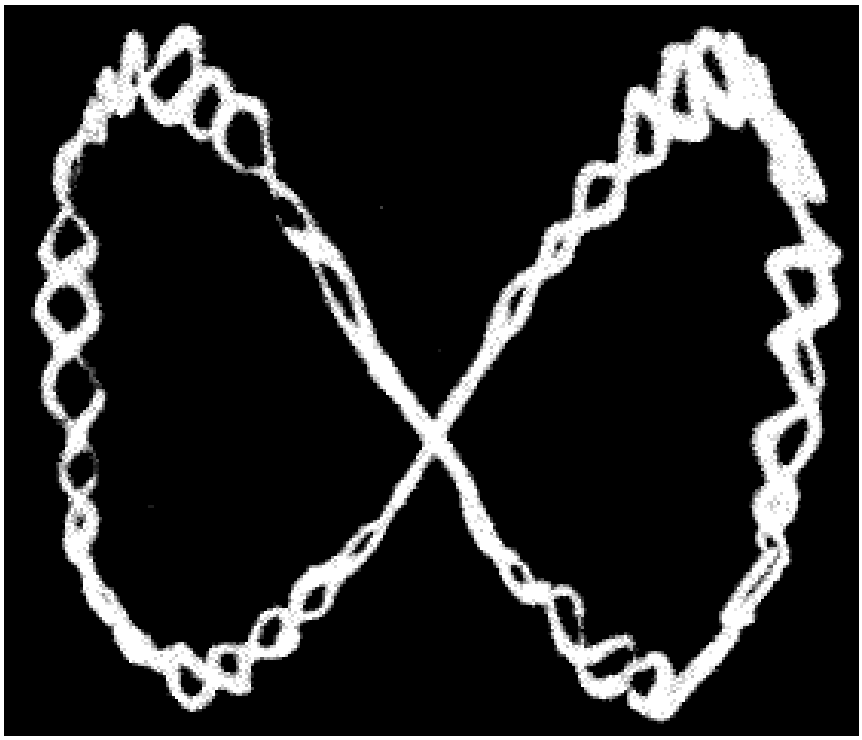

Figure 1-5. Ion motion in a quadrupole ion trap.[49]

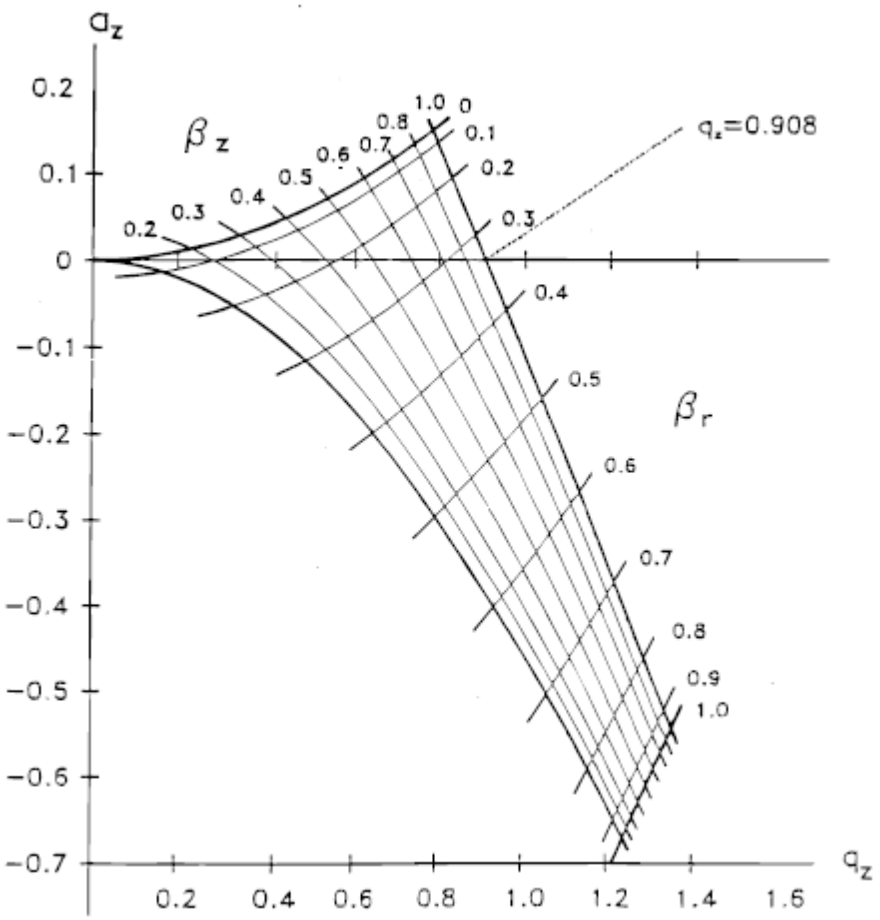

Figure 1-6. Mathieu stability diagram plotted in a and q space for positive ions. The shape of the stable region is rotated about the a_z =0 line for negative ions. Most commercial QITMS instruments operate along the a_z =0 line (RF-only operation). Under these conditions, ions will have a stable trajectory between q_z = 0 and 0.908. The β_z =1 boundary intersects the q_z axis at q_z = 0.908.[50]

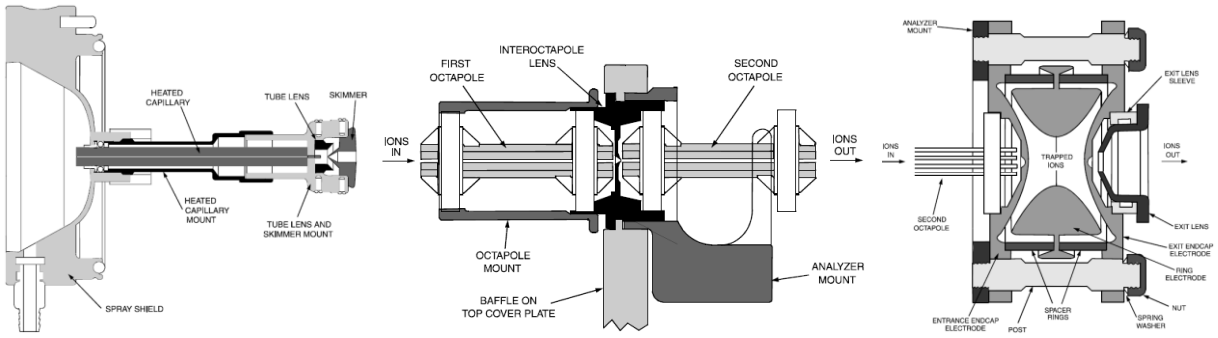

Figure 1-7. Schematic of Finnigan LCQ ion trap mass spectrometer.[48]

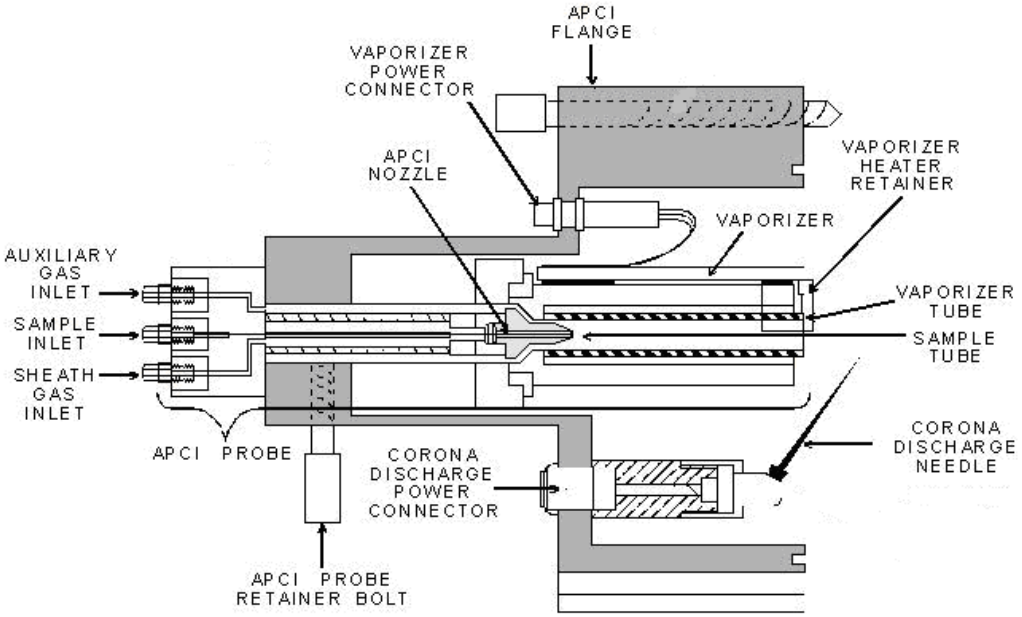

Figure 1-8. Schematic of the atmospheric pressure chemical ionization (APCI) source used in the LCQ.[48]

CHAPTER 2
FUNDAMENTALS OF FAIMS FOR CURVED ELECTRODE GEOMETRIES

Introduction

Buryakov et al. introduced FAIMS with a parallel plate geometry in 1993.[20] Since then, Carnahan et al. improved the sensor design by replacing the flat plates with concentric cylinders.[51] Spherical electrodes were also proposed but never reduced to practice.[52, 53] It has been theorized that curved geometries help to produce significantly better ion transmission efficiency because the electrode curvature allows unique ion focusing capabilities.[22, 23, 54] Ion losses in the analysis channel of planar electrodes arise mainly due to ion diffusion and space-charging. Krylov proposed a method to reduce diffusion losses by employing cylindrical electrodes in FAIMS.[22] With curved electrodes, there exists a non-uniform electric field. This electric field gradient points in the same direction as the vector of the compensating field,[22] and leads to a restoring force that acts on the diffusing ions, leading to compression of the ion cloud.

Although the use of curved surfaces increases sensitivity, resolution is compromised.[52] Decreased resolution is due to the ability of spherical or cylindrical surfaces to focus ions which encompass a wide range of mobilities. Since the non-uniformity of the field allows ions with a range of different mobilities to be focused together, they will exit the FAIMS cell at the same time, thus increasing peak width and decreasing resolution.

The development of novel hemispherical FAIMS electrodes to balance transmission and resolution has been pursued in this research. In a spherical or hemispherical cavity, all ions encounter equidistant trajectories from ion inlet to outlet, increasing focusing capabilities and transmission. The increased transmission can

allow the utilization of larger electrode radii, which will help to increase resolution. Figure 2-1 shows the novel hemispherical cell design and table 2-1 displays all relevant dimensions in comparison to the commercially available Thermo-Fisher Scientific cylindrical cell. An Ionalytics cylindrical cell was also employed in this research, as noted in table 2-1. The main difference between this cell and the Thermo-Fisher cell is the gap between the two electrodes (2.00 mm vs. 2.50 mm).

The strength of the focusing field between the two electrodes is inversely related to the radius of the electrodes. The smaller the radius of the electrodes, the stronger the focusing field will be; the larger the radius, the weaker it will be. A systematic exploration of the effect of electrode radius on sensitivity will be discussed in this research, with a comparison of the differences in sensitivity and resolution of the two cylindrical cells.

Description of Planar Geometry

Buryakov and others first introduced a parallel plate FAIMS geometry in 1993.[20] They showed that when an asymmetric waveform is applied to one of the plates while keeping the other plate grounded, a uniform electric field is created that allows for the transmission of only certain ions (figure 2-2). In this type of geometry, the ions are evenly distributed among the entire gap between the two electrodes. Ion losses in the gap of planar electrodes mainly come from lateral diffusion and space charging.

The motion of a positively charged ion in a flat plate FAIMS during the application of a hypothetical asymmetric waveform is displayed in figure 2-3. Ions are separated in FAIMS while they are carried by a continuous flow of gas between two closely spaced electrodes. The waveform employed by FAIMS is characterized by significant differences in voltage in the positive and negative polarities of the waveform. In figure

2-3 the mobility of a positive ion is higher during the positive (high voltage) portion of this waveform than during the negative (low voltage) portion. This ion will keep migrating towards the bottom electrode and be discharged if it remains on this path. A low direct current (DC) potential is superimposed to offset the drift of the ion. This DC potential is termed its compensation voltage (CV). The CV required to offset the drift of individual components in a mixture of compounds will be different if the change in the ions mobility between high and low field is different. Consequently, a mixture of compounds can be successfully separated by allowing each compound to transmit at its particular CV; scanning through these CV values creates a CV spectrum. The electric field (E_{flat}) between planar electrodes can be calculated using equation 2-1, where V_a is the applied voltage, and $(b-a)$ is the gap between the electrodes.

$$E_{flat} = \frac{-V_a}{(b-a)} \qquad 2\text{-}1$$

Description of Cylindrical Geometry

Curved geometry FAIMS was introduced by Carnahan and others in 1995.[51] A schematic of this geometry is displayed in figure 2-4. Curved geometry FAIMS is currently commercialized by Thermo-Fisher Scientific and is sold as a separation device to be used in tandem with a mass spectrometer. A schematic of the Thermo-Fisher cell is displayed in figure 2-5. The FAIMS process is the same as in a planar geometry - a mixture of ions may be filtered to one specific ion by selecting an appropriate compensation voltage. The difference arises when the application of an electric field is between curved surfaces. The field is no longer uniform and the non-uniformity of this field is what helps to focus the ions towards a fixed radial distance within the analyzer region. As more ions are focused towards the center, fewer ions are lost to the walls. In

essence, two-dimensional atmospheric-pressure ion focusing occurs within the analyzing gap.

The electric field (E_r) in a cylindrical geometry can be calculated at any point within the analyzer region by using equation 2-2

$$E_r = \frac{-V_a}{\left[r\ ln\left(\frac{a}{b}\right)\right]} \qquad 2\text{-}2$$

where V_a is the applied voltage, and as shown in figure 2-5, r is the radius of the ion at any point between the electrodes, a is the radius of the center electrode, and b is the radius of the distance between the center of the inner electrode and inner surface of the outer electrode.

Ion focusing in a curved geometry cell is achieved as ions near the inner electrode are repelled to the center of the analytical gap, and ions near the outer electrode are pulled back to the center of the analytical gap. Although ions experience a force that directs them towards a focus point it is important to note that the force is not necessarily strong, and the ions are distributed in space around this focus point due to the influences of diffusion, and ion-ion repulsions (space-charging).

This effect was experimentally described by Barnett et al. and is represented in figure 2-6. The CV that the ion needs to traverse the electrodes without being lost is displayed by the solid line. However, the variation in the electric field allows many ions with different CVs to be focused within the analyzer region. The electric field gradient for an example DV where the CV is the opposite polarity of the ion is represented by the dotted line $CV_{correct}$ in figure 2-6. The ions that are near the inner electrode (position of highest electric field) will be repelled away towards the center of the analyzer region where they will fall on the solid line and consequently be focused. Comparatively, ions

that are near the outer electrode will be pulled towards the center, where electric field is higher, and also be focused. Ions that would normally collide with either the outer electrode or inner electrode are represented by the dotted lines CV_{low} and CV_{high}, respectively. Since the field is not uniform and is higher near the inner electrode, the ion is pulled away from the outer electrode or inner electrode and successfully focused. Lastly, the dotted line $CV_{incorrect}$ displays an ion with a CV that, despite focusing, is not strong enough to deter the ions from the outer electrode.

While curved geometries in FAIMS increase transmission and thus sensitivity, they will decrease resolution. Since curvature aids in focusing a wide range of mobilities, peak widths will increase and resolution will decrease. The opposite is also true; if the radii of curvature is increased, the focusing effect lessens and resolution increases at the expense of sensitivity.

Each cell geometry has its advantages and disadvantages regarding the optimization of resolution and ion transmission due to the enhanced focusing that results in improved sensitivity. If the radius of curvature is decreased, focusing improves and ion intensity increases at the expense of resolution. Clearly, there is a compromise between resolution and transmission for both cylindrical and planar cell geometries. Thus it is interesting to consider geometries with curvature in both directions, i.e., spherical.

Description of Hemispherical Geometry

In a spherical cavity, all ions encounter equidistant trajectories from ion inlet to outlet, increasing its focusing capabilities, transmission, and uniformly spaced ion density. Nevertheless, the design and construction of a spherical cell is a daunting task; the suspension of a central spherical electrode at the exact center of a spherical cavity

while delivering several thousand volts of RF to the central electrode is extremely difficult.

Initial spherical designs failed to provide the precise, accurate, and rigid centering required of the center electrode. Therefore, a second design employed a hemispherical central electrode mounted within a hemispherical cavity, as shown in figure 2-1. This design has shown to provide the advantages of a fully spherical cell while permitting rigid, accurate, and reproducible positioning of the electrodes. Characterization and performance of the hemispherical FAIMS cell in comparison to the cylindrical cell will be reported.

The material of the inner electrode was stainless steel and was machined into a near hemisphere and fastened with metal screws to a Kel-F base plate. Kel-F, a polymer of chlorotrifluoroethylene, has the lowest vapor transmission rate of any plastic, excellent thermal characteristics and maintains an operating temperature range of -204 °C to 204 °C. Fastening the inner electrode to the base plate ensured accurate centering and a uniform analytical gap.

In order for the ions entering the analyzer region to ‘see’ a true hemispherical electrode, the inner electrode was extended 2 mm from a true hemisphere. This way, any path taken by the ions from inlet to exit would be identical. The asymmetric waveform and the compensation voltage were applied to the inner electrode through the mounting screw that was threaded in the center of the electrode (part 6 in figure 2-1). Photos of the hemispherical FAIMS cell are shown in figures 2-7 and 2-8.

The voltage (V_{hemi}) and the electric field (E_{hemi}) in a hemispherical geometry can be calculated at any point within the analyzer region by using equations 2-3 and 2-4

$$V_{hemi} = \frac{\Delta V}{\left(\frac{1}{b}-\frac{1}{a}\right)r} \quad 2\text{-}3$$

$$E_{hemi} = \frac{-V_a}{\left(\frac{1}{b}-\frac{1}{a}\right)r^2} \quad 2\text{-}4$$

where ΔV is the change in voltage, a is the inner electrode radius, b is the outer electrode radius, r is position, and V_a is the inner electrode voltage. In a planar cell, the electric field does not vary across the gap between the electrodes, as described by equation 2-1 and displayed by figure 2-9. The cylindrical cell, because of its curvature, is capable of focusing ions as described by equation 2-2 and displayed in figure 2-9 by the blue trace. In the cylindrical cell the field varies non-linearly and is higher at the inner electrode than the outer. The hemispherical cell offers higher sensitivity than that of the cylindrical geometry because of its curvature in both directions. The ions that are located at various radial distances between the inner and outer electrode of the hemispherical cell will more effectively fall into the atmospheric pressure ion trapping region because the focusing decreases ion loss to the walls.

Figure 2-9 displays how the electric field changes as a function of position for the three cells. As can be seen in the figure, the electric field for the hemispherical cell (green trace) is much higher near the inner electrode than for the other two geometries. This is important, for instance, for a cell that has the same dimensions and the same applied voltages. One would get more efficient separations without having to do any other modifications.

Description and Design of a Spherical Geometry

Guevremont et al. patented spherical electrodes in 2004, but the patent was never reduced to practice.[52] An initial design (figure 2-10) to suspend an inner electrode within a spherical cavity and not disrupt the electric field was constructed without any

success. The design (figure 2-10) included a spherical inner electrode that consisted of a 0.7 mm stainless steel rod drilled through the center of an 8.8 mm stainless steel ball. In order to deliver the asymmetric waveform and compensation voltage, the inner electrode needed to be suspended in this manner.

In order to minimize the disruption of the electric field within the analytical gap of the FAIMS cell, two MACOR sleeves (4 mm in diameter) were utilized to insulate the stainless steel rods. Minimization of any horizontal movement of the inner electrode was attempted by adding MACOR cuffs to the MACOR sleeves. The outer electrode was made of two adjoining brass hemispherical cavities held together tightly with thumb screws. The entire cell was encased in Delrin.

Unfortunately, this design was not successful. The primary reason for the poor transmission was probably imprecise centering of the electrode once the cell was assembled. Second, the MACOR sleeves used were very large in comparison to the size of the inner electrode. Ions entering the analyzer gap could theoretically be attracted to the insulating MACOR sleeves and lose their initial trajectory. Also, temperatures in excess of 150 °C were being used on the heated capillary of the MS. Delrin has an upper temperature limit of 175 °C.

As mentioned previously, the suspension of a central spherical electrode exactly at the center of a spherical cavity while delivering several thousand volts of RF to the central electrode is extremely difficult. Initial designs failed to provide the precise, accurate, and rigid centering required of the electrode. Thus, design of a novel spherical FAIMS cell incorporating a spherical central stainless steel electrode mounted

within a spherical stainless steel cavity that has been cut in half to allow for assembly was created.

This design has been shown to provide the ion optical advantages of a fully spherical cell while permitting rigid, accurate, and reproducible positioning of the electrodes. Characterization and performance of the spherical FAIMS cell shows an improvement in sensitivity and resolution when compared to the cylindrical FAIMS cell and will be discussed in this research.

A schematic, dimensioned cutaway drawing, and pictures of the novel spherical FAIMS cell are shown in figures 2-11 - 2-14, respectively. Both inner and outer electrodes are made of stainless steel. Outer casing is made of Ketron PEEK which is a polymer of polyetheretherketone. The melting point of Ketron is 340 °C. The asymmetric waveform and compensation voltage is applied by a stainless steel rod that has been drilled through the center of a 25.4 mm diameter inner electrode. A comparison table of important dimensions between all three cells (spherical, hemispherical, and Thermo- Fisher cylindrical) is displayed in table 2-2.

Experimental

Instrumentation

The instrumentation used in these experiments was a Thermo LCQ benchtop quadrupole ion trap mass spectrometer (Thermo-Fisher Scientific, San Jose, CA). The traditional sinusoidal waveform was created by either an Ionalytics GPI 1000 FAIMS system alpha prototype waveform generator or a Thermo-Fisher FAIMS waveform generator. Both generators run with a 33% duty cycle at a frequency of 750 kHz. The voltages for the waveform, compensation voltage, outer electrode, and curtain plate are all supplied by these two waveform generators. The Ionalytics generator required the

compensation voltage to be scanned using an external Agilent 33120-A arbitrary waveform generator, (Loveland, CO). The Agilent generator is programmed to generate linear voltage ramps in either positive or negative directions to scan the compensation voltage. The Thermo-Fisher generator provided the CV ramp so no external generator was required. Negative ions were created by atmospheric pressure chemical ionization (APCI). Analyte samples were infused at 15 µL/min.

The LCQ does not require any modification to the interface for attachment of the FAIMS assembly. A PEEK adapter was fitted onto the portion of the heated capillary that extends beyond the API stack spray shield (figure 1-7). The FAIMS cell is fitted into the PEEK adapter. The carrier gas used in the FAIMS apparatus, nitrogen (N_2), was passed through an individual gas purification cartridge equipped with molecular sieves for removal of moisture and activated charcoal for removal of organic impurities. Flow rate for nitrogen was controlled by an MKS M100B thermal mass flow controller (Andover, MA) calibrated for the individual gas.

Samples

For these experiments, several structural classes of common explosives were utilized (shown in figure 2-15), including nitroaromatic explosives such as 2,4,6-trinitrotoluene (TNT), 1,3,5-trinitrobenzene (TNB), 2,4-dinitrotoluene (2,4-DNT), and 1,3-dinitrobenzene (1,3-DNB), 3,4-dinitrotoluene (3,4-DNT); nitramine based explosives such as 1,3,5-trinitroperhydro-1,3,5-triazine (RDX) and 1,3,5,7-Tetranitro-1,3,5,7-tetraazacyclooctane (HMX); and nitrate esters pentaerythritol tetranitrate (PETN) and 1,2,3-propanetriol trinitrate (nitroglycerin, NG). Explosive standard solutions were supplied by Dr. Yehuda Yinon of the Weizmann Institute of Science (Analytical Laboratory, Israeli Police Headquarters).

Negative ion mode was employed since the above explosives tend to display high electron affinities. Furthermore, less chemical noise is generated in negative ion polarity mode thus increasing the selectivity of the analysis.[48] In APCI, negative ions are typically produced by proton abstraction to obtain an $[M-H]^-$ ion[55] except for TNT, TNB, and DNT isomers which produce mostly the $[M]^-$ ion plus other common fragments.

All explosive solutions were diluted in a solvent mixture consisting of 65% methanol and 35% deionized water (65:35, v/v). Utilizing a combination of methanol and water as a solvent allows the use of lower vaporizer temperatures with the APCI ion source to avoid the degradation of fragile explosive analytes. Additionally, approximately 0.1% of carbon tetrachloride was added for nitramine and nitrate ester based explosives. The addition of carbon tetrachloride allows a stable explosive adduct ion, $[M + Cl]^-$, to be formed. Anticipated ions and adducts for nitramine and nitrate ester explosives are shown in table 2-3. For these experiments, all solutions were diluted to a concentration of 10 ppm unless otherwise noted.

Results and Discussion

A mixture of explosives, as well as individual analyte solutions, was tested with each geometry to evaluate signal intensity, compensation voltage, resolution and resolving power. The resolution between peaks in a mixture can be evaluated by equation 2-5.

$$R_s = \frac{2(\Delta CV)}{(PW_{1\,10\%} + PW_{2\,10\%})} \qquad (2\text{-}5)$$

where ΔCV is the difference in CV values of the two peaks and PW_1 and PW_2 are the full width at 10% of peak 1 and 2, respectively. The resolving power for FAIMS ($R_{p\ FAIMS}$) is an instrumental parameter described by equation 2-6

$$R_{p\ FAIMS} = \frac{CV}{PWHM} \tag{2-6}$$

where CV is compensation voltage and $PWHM$ is the peak width at 50% peak height. The CV of any particular ion is calculated by using equation 2-7.

$$CV = \left[\frac{peak\ \ time}{total\ \ scan\ \ time} * scan\ range\right] - \ start\ of\ scan \tag{2-7}$$

Comparison of Signal Intensity

The spatially inhomogeneous field in curved geometry FAIMS not only separates ions but also focuses the ions that are at their correct CV values. Thus, the transmission of ions increases with increasing curvature. Figure 2-16 shows a CV scan (figure 2-16, left) and mass spectrum (figure 2-16, right) of TNT for all three (cylindrical, hemispherical, and spherical) FAIMS cells. Note that these set of experiments were done with the cylindrical FAIMS cell that has a 2.00 mm gap (Ionalytics cell). Separation parameters for all three cells include: DV of -3214 with a CV scan from 0 to +10 V over 2 minutes (5 V/min). The CVs of TNT for all three cells are all ~4.60 V. Signal intensity for the hemispherical FAIMS shows eight-fold increase from that of the cylindrical cell. The spherical FAIMS cell gave an intensity which is a 23-fold increase from the cylindrical cell. The negative APCI spectrum of TNT shows the production of $[M]^-$ at *m/z* 227. The mechanism that occurs with APCI with TNT is assumed to be electron capture since TNT has three bulky electron-withdrawing nitro groups.[56, 57] All three TNT spectra also display two low-intensity fragment ions, $[M\text{-}NO]^-$ at *m/z* 197 and $[M\text{-}OH]^-$ at *m/z* 210, which may form during the transition of the ion from atmospheric

pressure to vacuum through the heated capillary or in the tube lens – skimmer region where ions are declustered from solvent vapor.

This behavior of increasing intensity with increased FAIMS electrode surface area was verified with TNB and 2,4-DNT, as displayed in figures 2-17 and 2-18, respectively. For figure 2-17 the separation and scanning parameters include: DV of -3214 with a CV scan from 0 to +10 V over 2.5 minutes (4 V/min). The CVs of TNB for all FAIMS cells are ~6.10 V. Signal intensity for the spherical FAIMS cell (7.50×10^5) shows a 13-fold increase from the cylindrical FAIMS and the hemispherical FAIMS shows a 3-fold increase from the cylindrical cell. The negative APCI spectrum of TNB is shown in figure 2-17 and it displays the major ion as *m/z* 213, $[M]^-$. The major fragment that is produced in all three spectra is *m/z* 183, $[M\text{-}NO]^-$. Figure 2-18 shows a compensation voltage scan and a mass spectrum of 2,4-DNT for all three cells. Separation and scanning parameters are the same as with TNB. The CVs of 2,4-DNT for all three cells is ~7.50 V. Signal intensity for the hemispherical FAIMS shows a 5-fold increase from that of the cylindrical cell. The spherical FAIMS cell gave an intensity value of 7.27×10^5 which is 17-fold increase from the cylindrical cell. The APCI spectrum of 2,4-DNT for all three cells show the molecular ion at *m/*z 181 $[M]^-$ and its major fragment at *m/*z 135 $[M\text{-}NO_2]^-$. This experiment was repeated for several other explosives including RDX, HMX, NG, and PETN. Table 2-4 shows these results. Note that the values in table 2-4 were taken as three repetitions of the compensation voltage scan. The average of the centroid peak and the standard error of standard deviation of the mean (S_E) is reported in the table. Unfortunately, HMX and NG were not able to be detected with any of the FAIMS cells while scanning the compensation voltage. This can be

attributed either to not scanning the CV slowly enough to be able to detect the analyte peak or to the fragility of these ions causing the molecular ion to fragment before it reached the ion trap.

An investigation of curved geometry FAIMS electrodes has shown that higher signal intensity is achieved with the spherical and hemispherical cells. It is assumed this is due to the two-dimensional focusing within the analytical gap of these cells. The stronger the curvature is (when comparing between cylindrical and both the hemispherical and spherical), the more powerful the electric field gradient will be and, thus, the better the sensitivity. It should be noted that even though the hemispherical and spherical cells have the same radius of curvature, they obtained different intensity values. One would assume that a cell with the same radius of curvature should provide identical sensitivity values. The higher sensitivity of the spherical cell could be due to its larger surface area since that is the only real notable difference between the two cells. Further studies with cells of different dimensions, would need to be performed in order to verify this assumption. It should also be noted that there is no significant difference in compensation voltage within the three CV scans of each cell, exemplifying the reproducibility of the hemispherical and spherical FAIMS cells.

Comparison of Resolving Power and Resolution

Figure 2-19 displays one CV scan of a 2 ppm mixture of TNT, TNB, 2,4-DNT, 1,3-DNB, and PETN on the Thermo-Fisher cylindrical cell (2.50 mm gap). The total ion current (TIC) is shown in (A). Intensities of TIC and extracted chromatograms, $R_{p\,FAIMS}$, and CVs are also shown in figure. The compensation voltage for figure 2-19 was scanned from -5 to +15 V over 2 minutes (10 V/min) with a dispersion voltage of -4000 V. This dispersion voltage corresponds to an electric field of 16,000 V/cm or 80

Townsend (Td). A Townsend is a unit of the *E/N* ratio, where *E* is the electric field and *N* is the gas number density (1 Td = 10^{-17} V cm^2). The same explosives mixture was analyzed on the hemispherical (figure 2-20) cell. Hemispherical cell scanning parameters include a dispersion voltage of -3214 V and a CV scan from -1 to +19 V over 2 minutes (10 V/min). This dispersion voltage corresponds to an electric field of 16,072 V/cm and/or 81Td. Even though the absolute scanning range of the Thermo-Fisher cylindrical cell and the hemispherical cell are not identical, the rate of scanning (10 V/min) is the same. Resolution between peaks was calculated using equation 2-5. Resolution and resolving power values are clearly higher for the hemispherical cell. The higher resolution in the hemispherical cell can be attributed to its bigger inner electrode radius and better focusing capabilities. The radius is twice the size of the cylindrical cell, giving it a more planar-like feature, thus increasing its resolution. Also, the path length through the cell is ~2x longer which gives 2x longer residence time, and thus 2x more RF cycles. The bigger inner electrode radius allows for increased resolution with increased transmission.

The same explosives mixture was attempted on the spherical cell, the results are shown in figure 2-21. The scanning parameters for the spherical cell include a compensation voltage scan from -1 to +19 V over 2 minutes (10 V/min) with a DV of -3214 V. As seen above, the spherical FAIMS displays an improvement in sensitivity (typically ~4x) for each of the extracted chromatograms and TIC compared to the hemispherical cell. Note also that the spherical cell exhibits a ~2x decrease in resolving power and resolution from the hemispherical cell. Again, this could be attributed to its larger surface area. A larger surface area gives a higher potential for distortion of the

electric field which, in turn, could prevent the ion cloud to exit the cell at the appropriate time and thus broaden its peak width. Another possible explanation for the sphericals' lower resolution could be longer theoretical residence times within the analyzer region. The residence time of the ion denotes how long that ion remains within the gap before exiting towards the mass spectrometer. The *calculated* residence times for the spherical and the hemispherical cell are identical (114 ms) but the ion does have a larger surface area within the spherical cell which could increase its trajectory time. Theoretically, if the ion has a longer trajectory and remains in the gap for a longer time its peak width will be broader as it exits the cell. Tables 2-5 and 2-6 illustrate specific figures of merit for all three cells to fully compare them.

In order to evaluate whether these trends were affected by dispersion voltage, another 2 ppm mixture including TNT, TNB, 3,4-DNT, 2,4-DNT, and 1,3-DNB was attempted with all three cells at a higher dispersion voltage. These experiments were performed with the Ionalytics cylindrical cell (2.00 mm gap). The scanning parameters for all three cells included a dispersion voltage of -4700 V (23,500 V/cm) with a compensation voltage scan from 0 to +20 V over 4 minutes (5 V/min). These results are displayed in figures 2-22 (cylindrical), 2-23 (hemispherical), and 2-24 (spherical). Resolving powers, CVs, and intensities for the chromatograms are shown on each figure. The figures of merit for the three cells at 4700 DV are compared in tables 2-7 and 2-8. As in the lower dispersion voltage experiments, spherical FAIMS displayed an improvement in sensitivity but a decrease in resolution when compared to the hemispherical cell. Even though the resolution and resolving power values were lower for the spherical cell at both dispersion voltages, they still showed an improvement from

both the two cylindrical cells. Attempting to maximize both resolution and sensitivity is dependent upon how well the incorporation of both 'planar-like' and 'curve-like' qualities of the cell are employed.

Sensitivity of Spherical FAIMS

Since FAIMS is able to separate analyte ions from chemical background noise and thereby enhance selectivity, an evaluation of the analytical capabilities of the spherical FAIMS cell was carried out in this research. Evaluation of CV repeatability, linear dynamic range, and limit of detection for the explosive TNT was performed.

Repeatability of compensation voltage in FAIMS is a crucial parameter that describes the consistency of the analytical approach. A repeatable compensation voltage is similar to a reproducible retention time in chromatography and can be treated as a verifiable index of identifying the explosive compound. The repeatability of CV value was tested at ten different dispersion voltage values each with five repetitive injections of a 10 ppm TNT sample while employing the same conditions over a period of several hours. Standard deviations (SDs) and relative standard deviations (RSDs) were calculated by analysis of variance. As shown in table 2-9, better repeatability was obtained at higher dispersion voltages and this is assumed to be due to the increased ion focusing and thus increased ion transmission of analyte ions. This results in a more symmetrical and intense CV peak, which in turn, generates more precise and reproducible CV values.

In order to fully validate the spherical FAIMS method, limit of detection (LOD) and linear dynamic range were also characterized. LOD describes the lowest concentration level of the analyte that may be determined to be statistically different from a blank sample.[58] In this research, the method validation values are reported in a format

consistent with the International Union of Pure and Applied Chemistry (IUPAC) definitions. The LOD was taken as three times the standard deviation of the blank signal, expressed in concentration. Blanks in this research are defined as infusing the solvent solution (with no analyte) while scanning the mass spectrometer for similar times as actual runs. The signal intensity of blanks were averaged and utilized for statistical analysis. Solutions were flowed at 15 µL/min at concentrations of 0, 1, 10, 50, 100, 250, 500, 1000, and 10000 ng/mL (1 ppb to 10 ppb) were made and the mass spectrometer was scanned in the full-scan and selected ion monitoring (SIM) mode. The CV was scanned from 0 to +10 V over two minutes (5 V/min). Linear dynamic range (LDR) was evaluated by five replicate injections of standard mixtures at eight different levels of concentration ranging from 1 ppb to 10 ppm. The lowest point of quantitation, specifically, the concentration yielding a signal that is ten times the standard deviation of the blank. The highest point refers to the highest concentration that shows a linear dependence of the intensity on concentration. Results of these experiments are shown in table 2-10. Based on the data shown, the LOD of TNT collected in full scan MS was 4 ng/mL and was 1 ng/mL in SIM mode. The correlation coefficient (r^2) value for the regression was 0.9951 for full scan and 0.9968 for SIM mode, demonstrating a LDR of ~3 orders of magnitude for the FAIMS analysis of TNT. Even though higher LODs and lower correlation coefficients were obtained with full scan, it is still a vital mode for research analysis as more information about molecular and fragment ions is provided.

FAIMS separation is based on a different principle than chromatography, even though it provides chromatogram-like data. In contrast to liquid or gas chromatography,

where the analytes pass through the column over a window of retention times and are detected, FAIMS can be used to allow only specific analytes to traverse the cell by setting a particular compensation voltage. Thus, FAIMS/MS is more analogous to MS/MS than to GC/MS or LC/MS.

Conclusions

In this chapter, an investigation of three-dimensional and two-dimensional curved electrodes with respect to signal intensity, resolution, and resolving power was shown. Although the use of curved surfaces increases sensitivity, resolution is decreased. Decreased resolution is due to the ability of cylindrical, hemispherical, or spherical surfaces to focus ions which encompass a wide range of mobilities. Since the non-uniformity of the field allows ions with different mobility behaviors to be focused together, they will exit the FAIMS cell at the same time, thus increasing peak width and decreasing resolution. This effect is more pronounced with increasing curvature and/or surface area as was displayed in the data. To balance transmission and resolution, the development of novel hemispherical and spherical FAIMS electrodes were employed in this research.

The highest sensitivity for the explosives was obtained with the spherical FAIMS electrode. Additionally, the spherical FAIMS electrode allowed better resolving power and resolution values than both the Thermo-Fisher cell cylindrical (2.50 mm gap) and the Ionalytics cylindrical cell (2.00 mm gap). The increased transmission allows the utilization of larger electrode radii, which can help to increase resolution.

The sensitivity of spherical FAIMS was explored to provide information on its quantitative capability. The best CV repeatability was obtained at higher dispersion voltages (-2000 to -3378 V). The standard deviations for TNT ranged from 0 to 0.04

and the relative standard deviations ranged from 0 to 2.3%. Two MS scan modes, full-scan, and SIM, were tested for LOD and LDR. Limit of detection for TNT was 4 ppb for full scan and 1 ppb for SIM. Although full-scan MS provided higher LOD and LDR values, it is still a vital explosive analysis mode because it provides more information about the ion.

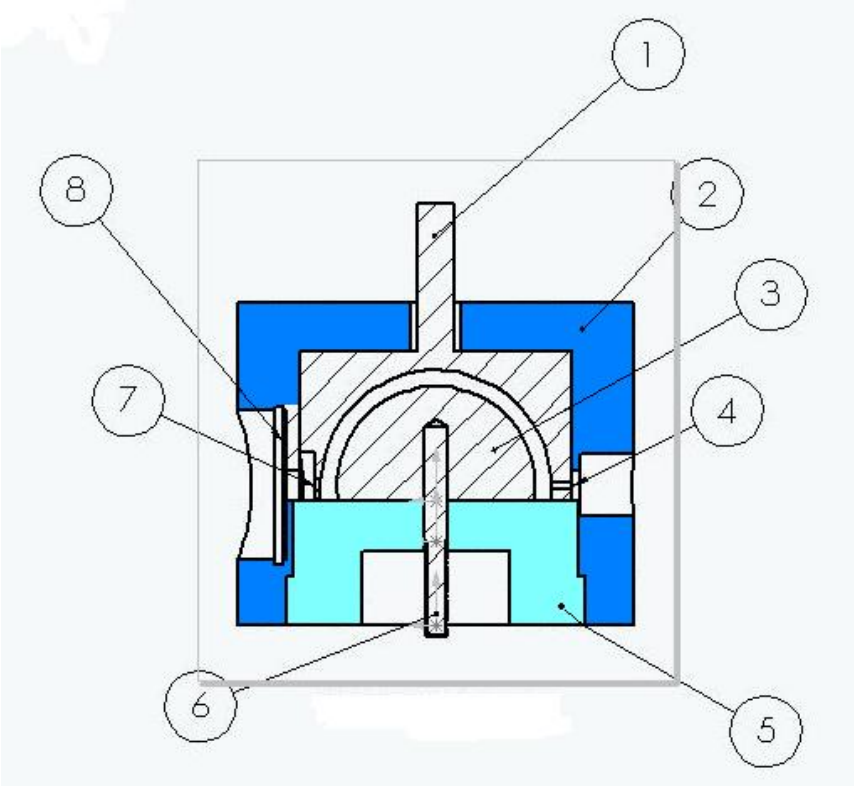

Figure 2-1. Schematic of hemispherical FAIMS electrodes. (1) outer electrode, (2) outer housing, (3) inner electrode, (4) exit port, (5) base, (6) inner electrode connection, (7) entrance port, and (8) curtain plate.

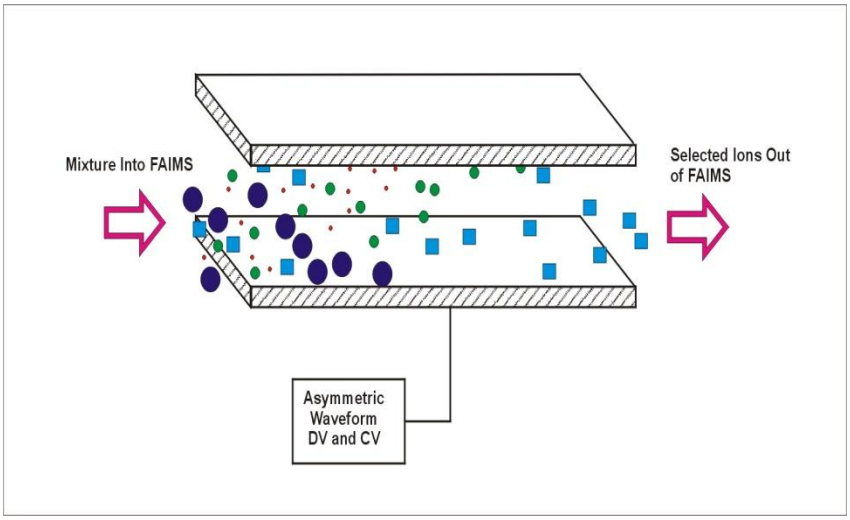

Figure 2-2. Ions separated between flat plates in the FAIMS analyzer. The transmitted ion is distributed evenly over the gap between the plates. Ions are continuously lost through diffusion and space charge repulsion. [59]

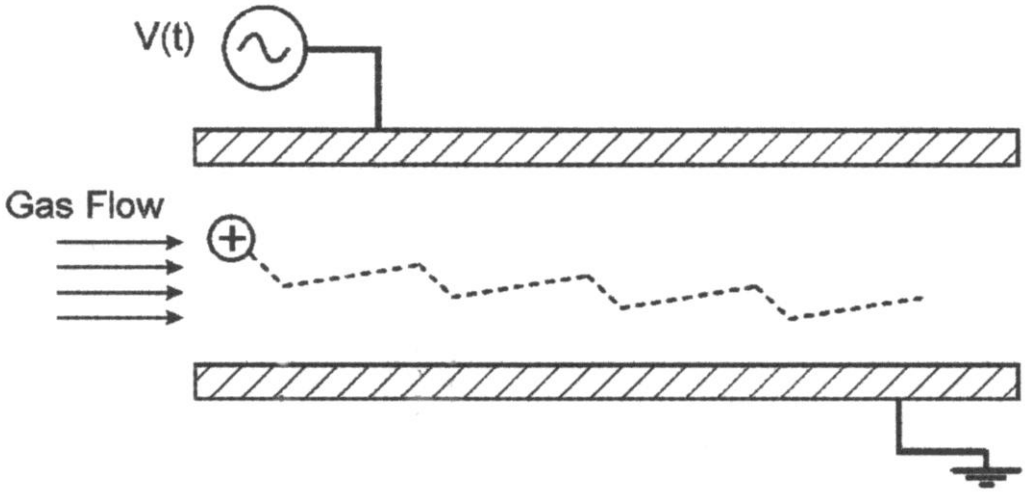

Figure 2-3. Motion of a positively charged ion in a flat plate FAIMS.[21]

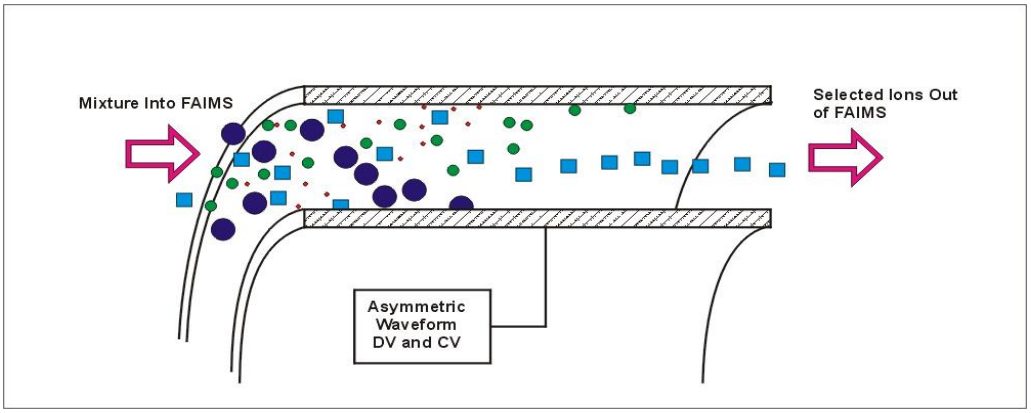

Figure 2-4. Ions separated between concentric cylinders of a FAIMS analyzer. The transmitted ion is focused towards a fixed radial distance, and distributed around that distance through the effects of diffusion and space charge repulsion. The effect of the focus is exaggerated for clarity in this figure.[59]

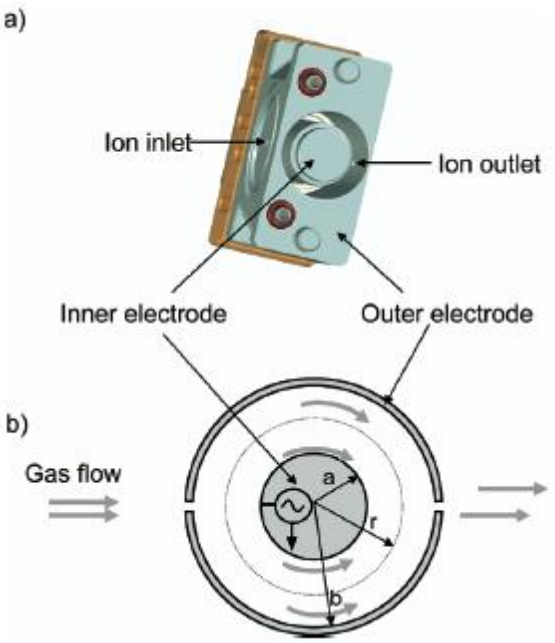

Figure 2-5. Three-dimensional schematic and cross section of the Thermo-Fisher cylindrical geometry FAIMS. (a) Three-dimensional view and (b) cross section view illustrating radial location, r, between the walls of the inner electrode, 'a' and outer electrode 'b'. The asymmetric waveform is applied to the inner electrode.[60]

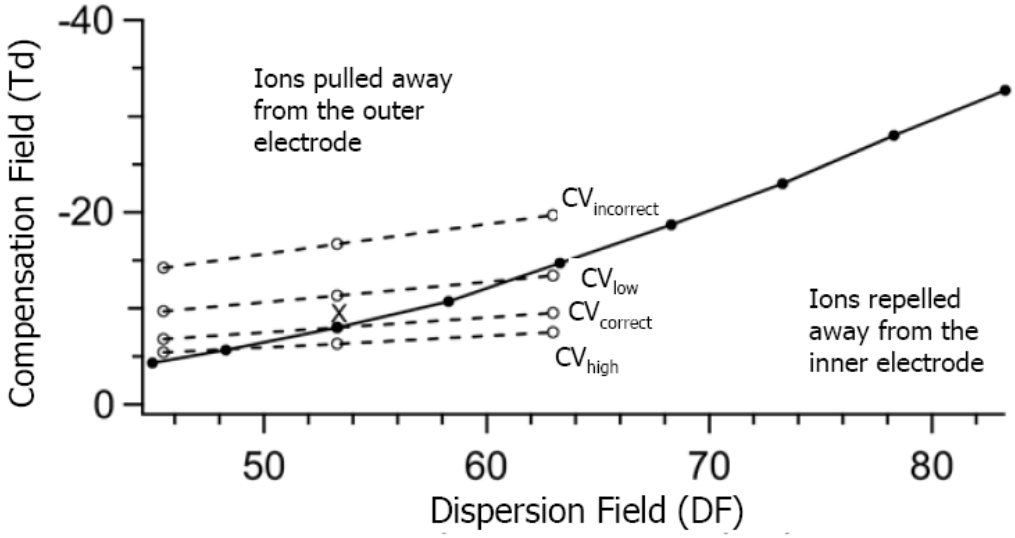

Figure 2-6. Focusing effect caused by curvature of electrodes in FAIMS. Adapted from Barnett et al.[60]

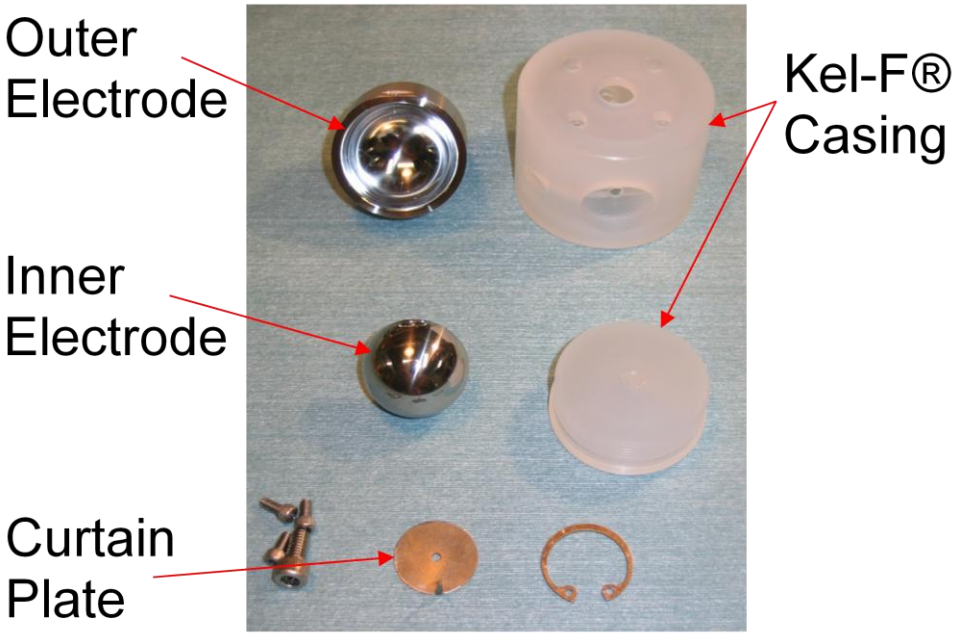

Figure 2-7. Disassembled hemispherical FAIMS cell.

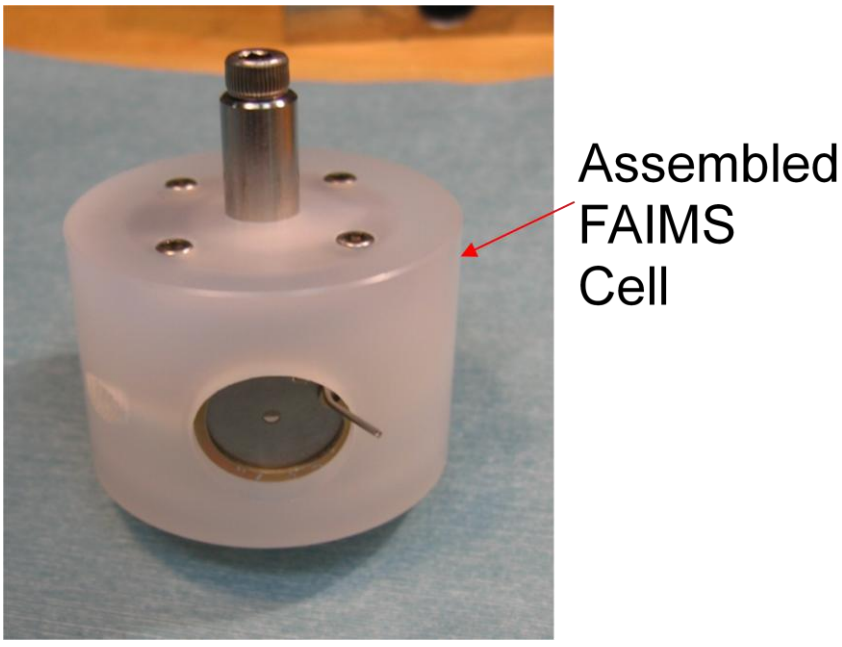

Figure 2-8. Assembled hemispherical FAIMS cell. Outer casing is made of Kel-F and curtain plate is made of stainless steel.

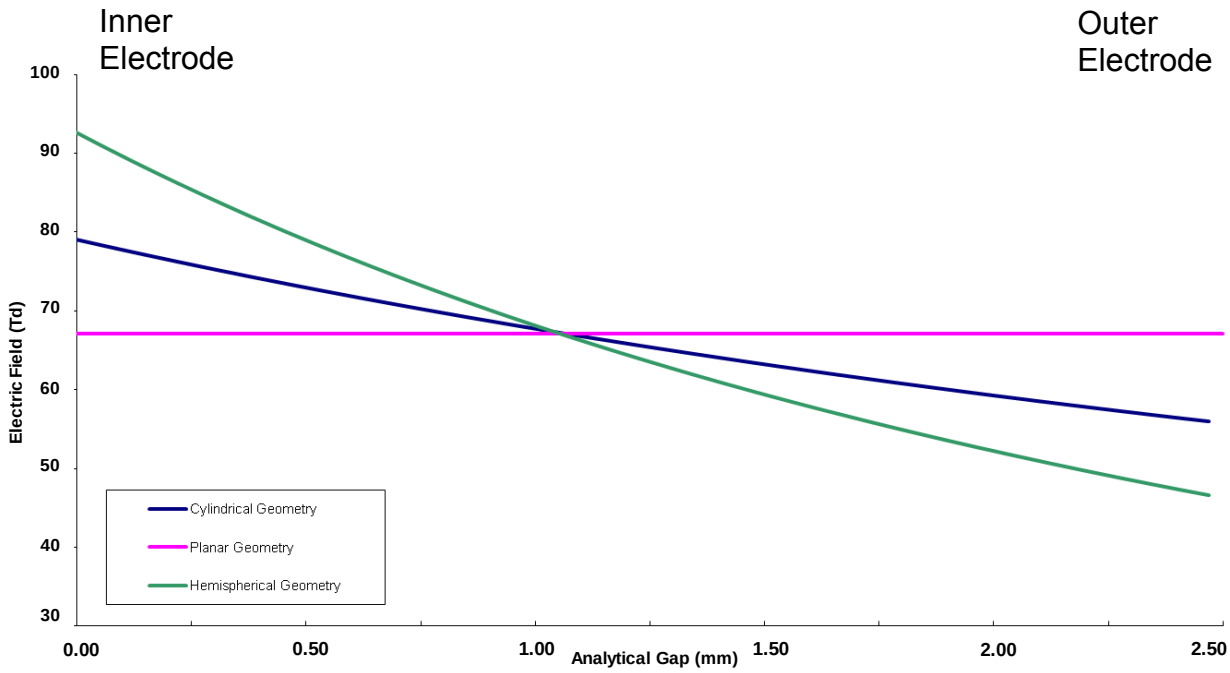

Figure 2-9. Variation of the electric field as a function of position for the three FAIMS cells. All three cells contain a gap of 2.50 mm. Radius of inner electrode for cylindrical and hemispherical is 6.00 mm. DV for all three is 4000 V.

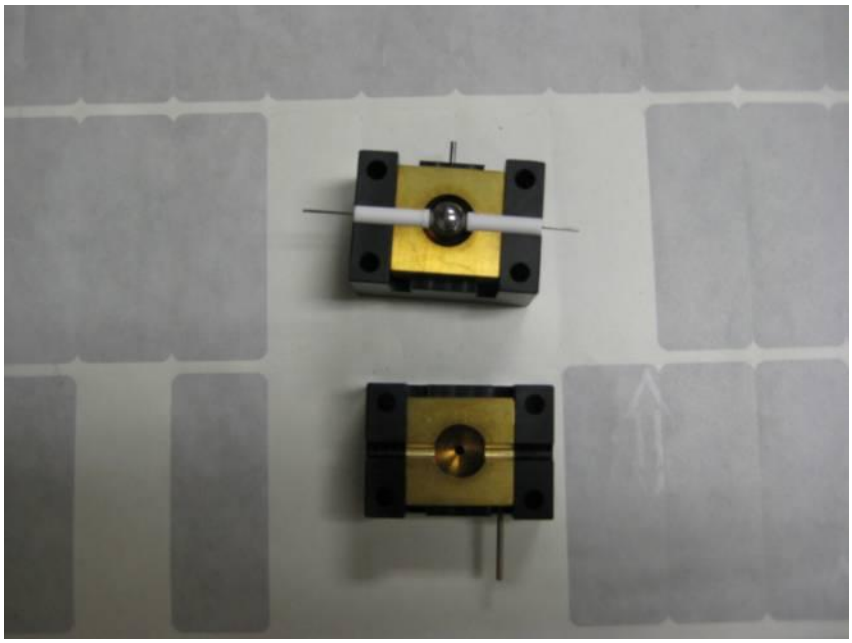

Figure 2-10. Original spherical FAIMS design. Outer casing is made of Delrin, electrodes of brass, and inner electrode of stainless steel.

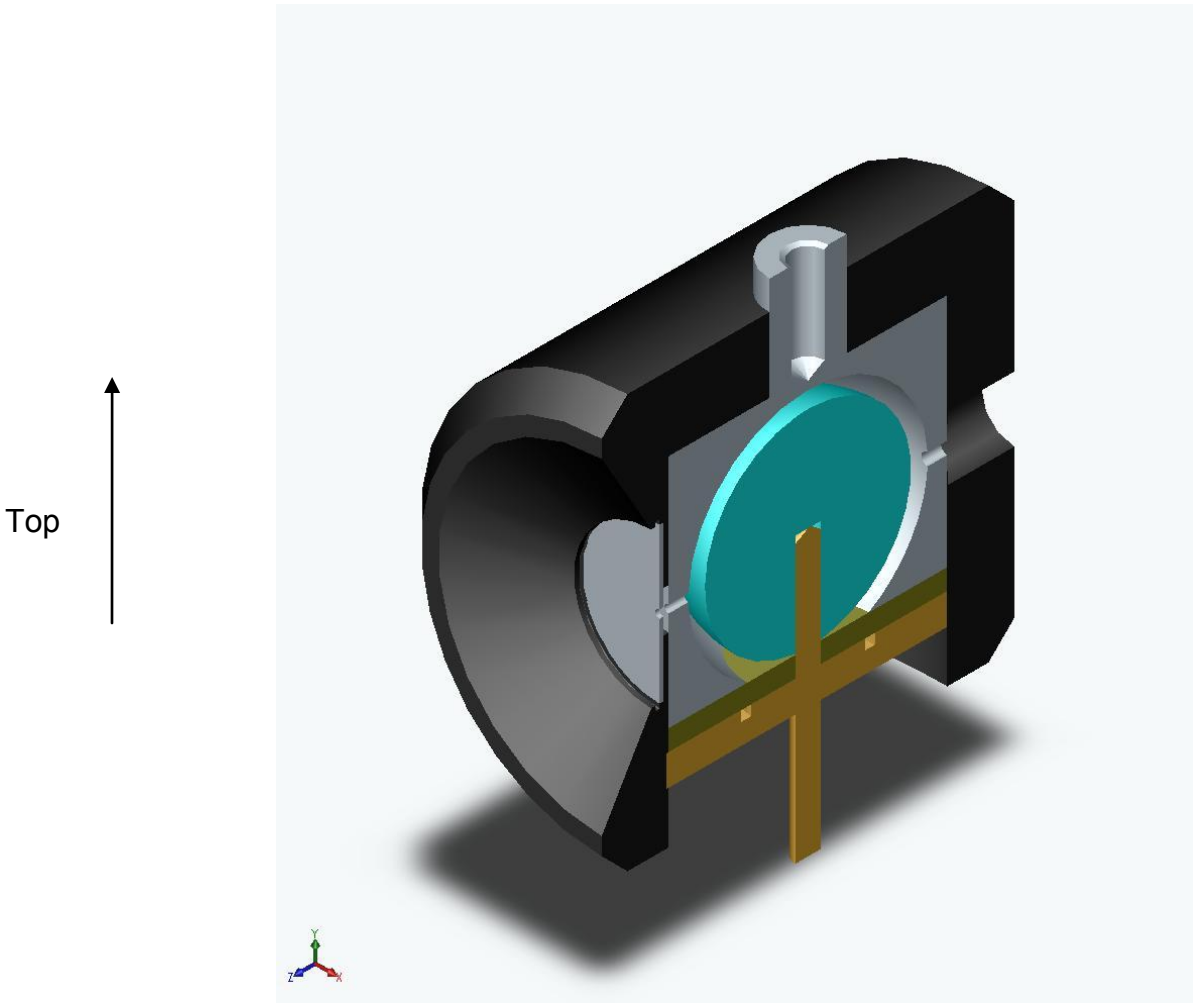

Figure 2-11. Novel spherical FAIMS cell. Outer casing is made of PEEK, inner and outer electrodes are made of stainless steel.

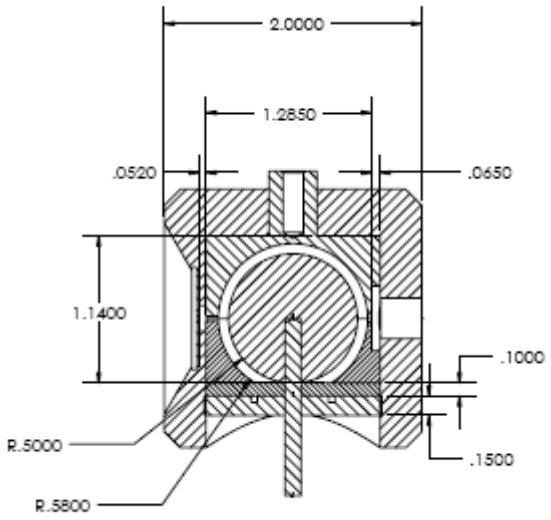

Figure 2-12. Dimensions of novel spherical FAIMS cell (in inches).

Figure 2-13. Disassembled spherical FAIMS electrodes. Both inner and outer electrodes are made of stainless steel.

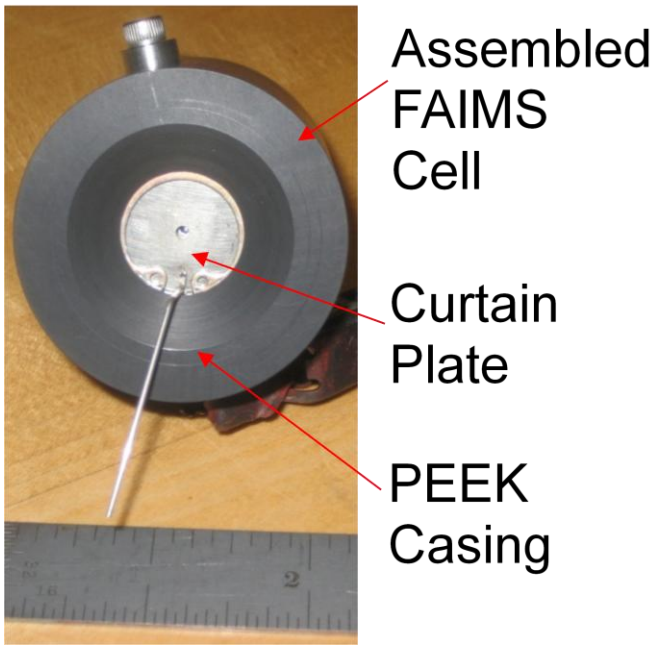

Figure 2-14. Assembled spherical FAIMS cell. Outer casing is made of Ketron PEEK. Curtain plate is made of stainless steel.

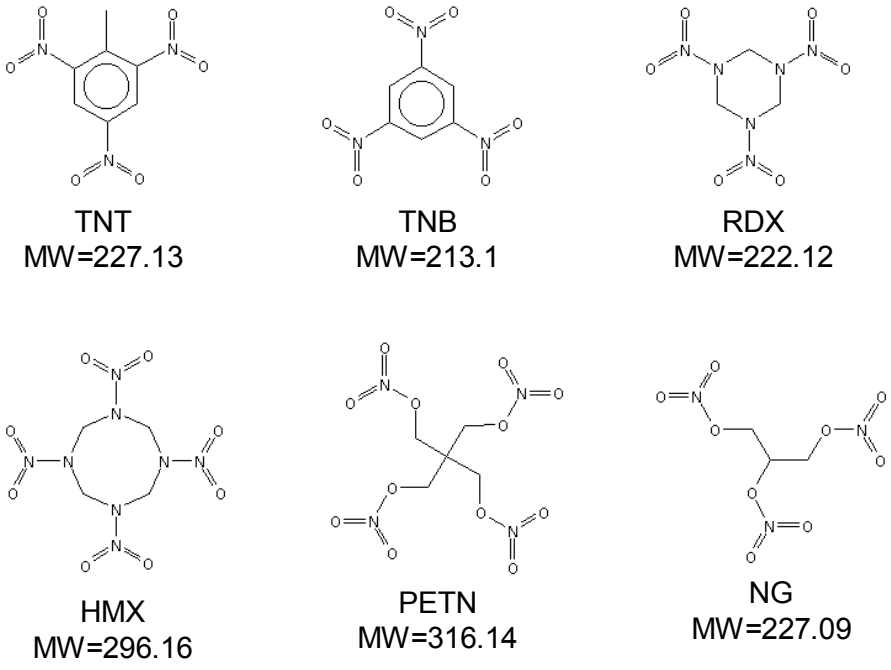

Figure 2-15. Structures of several structural classes of common explosives studied in this work.

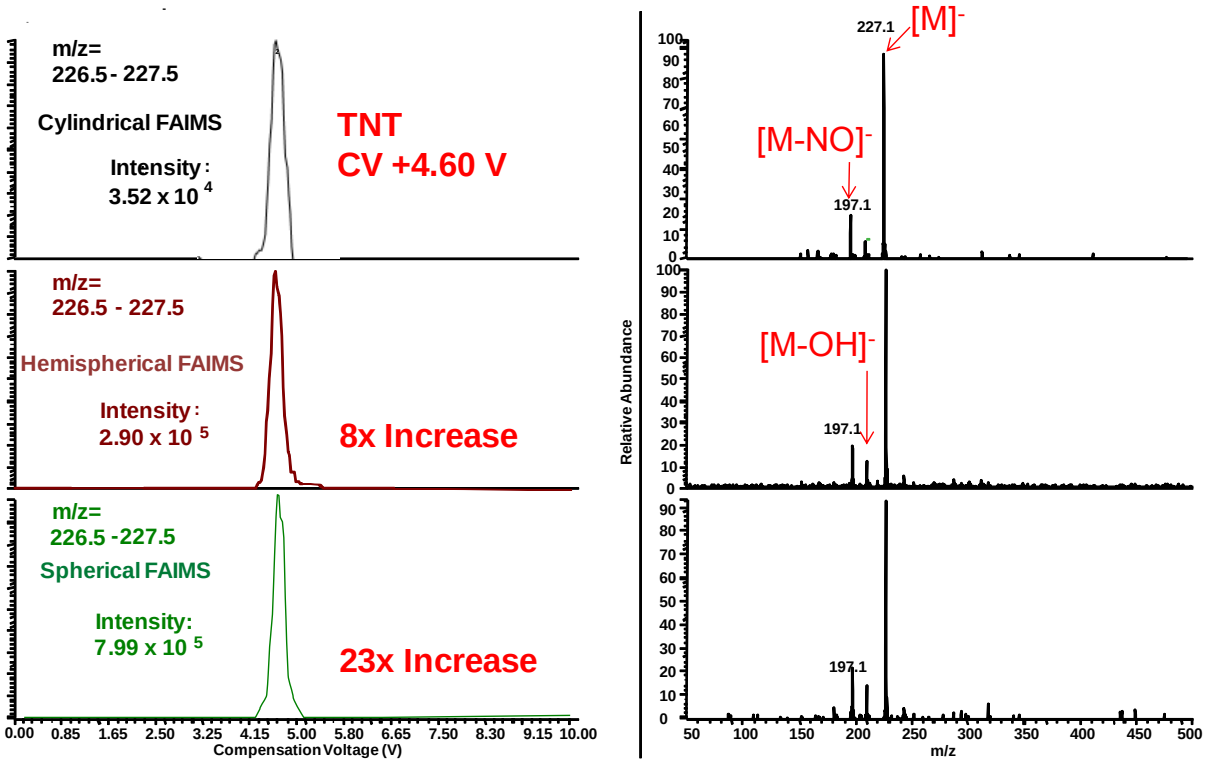

Figure 2-16. Comparison of signal intensity of TNT between all three FAIMS cells. Extracted chromatogram of *m/z* 227 on left and corresponding mass spectra on right. Ionalytics cylindrical FAIMS (top), hemispherical FAIMS (middle), and spherical FAIMS (bottom).

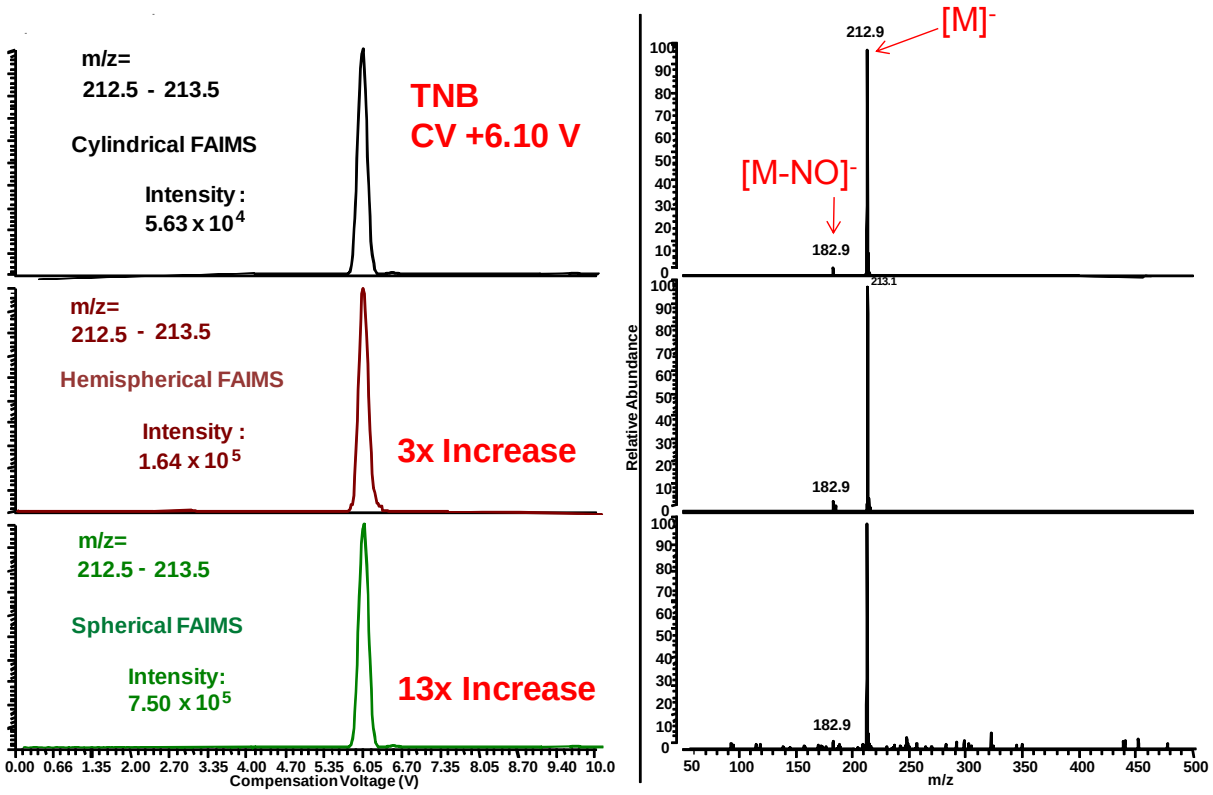

Figure 2-17. Comparison of signal intensity of TNB between all three FAIMS cells. Extracted chromatogram of *m/z* 213 on left and corresponding mass spectra on right. Ionalytics cylindrical FAIMS (top), hemispherical FAIMS (middle), and spherical FAIMS (bottom).

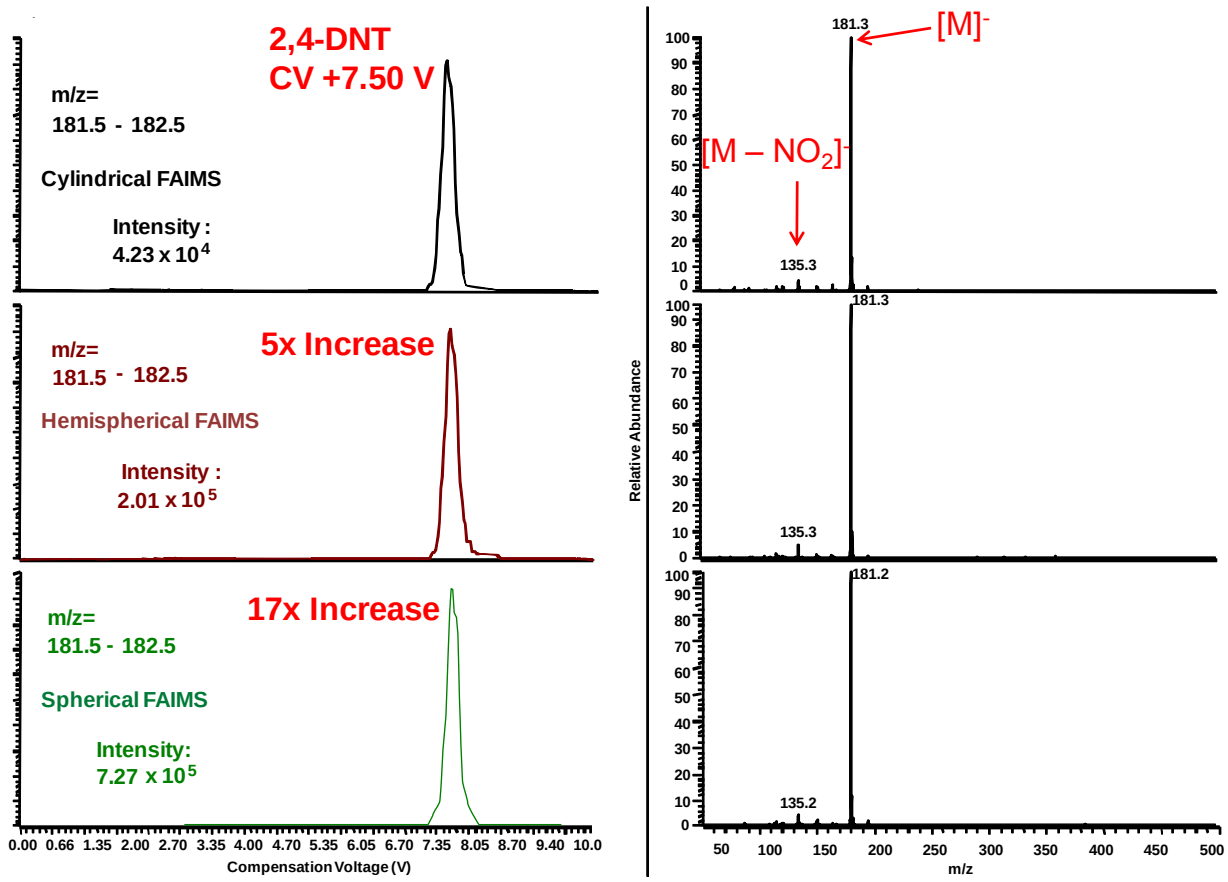

Figure 2-18. Comparison of signal intensity of 2,4-DNT between all three FAIMS cells. Extracted chromatogram of *m/z* 182 on left and corresponding mass spectra on right. Ionalytics cylindrical FAIMS (top), hemispherical FAIMS (middle), and spherical FAIMS (bottom).

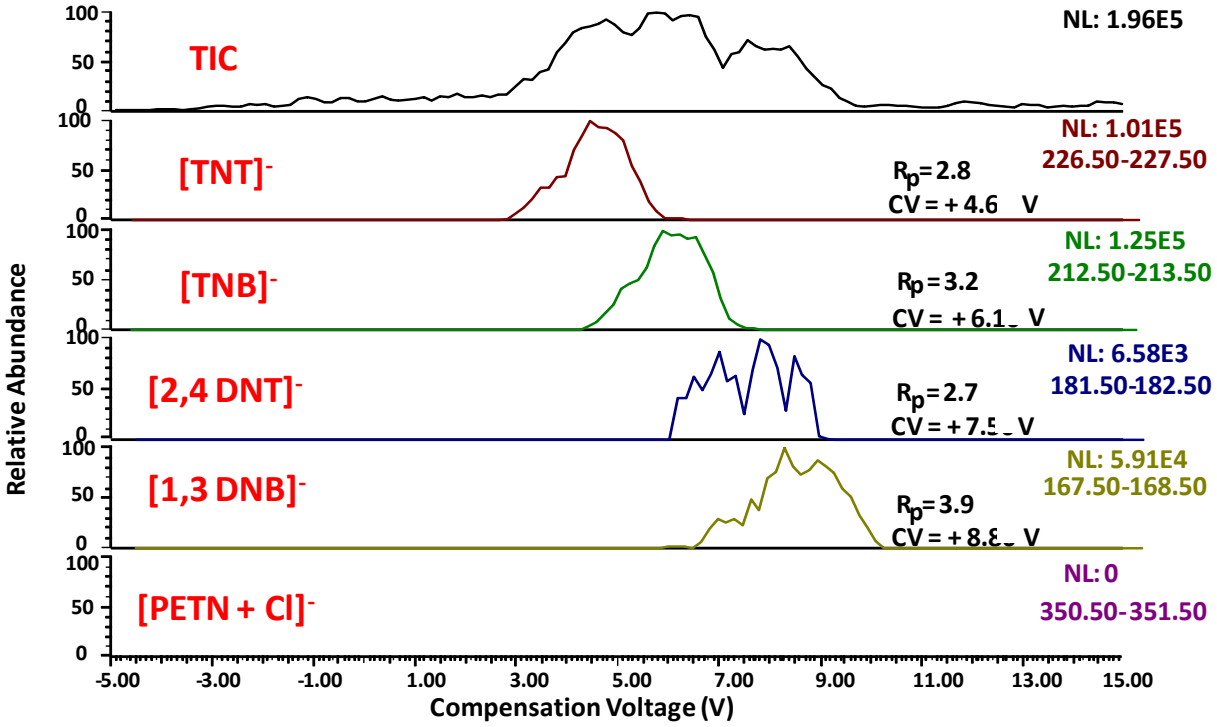

Figure 2-19. CV scan of a 2 ppm mixture of explosives on the Thermo-Fisher cylindrical cell at a DV -4000 V. (A) TIC, (B) TNT, (C) TNB, (D) 2,4-DNT, (E) 1,3-DNB, and (F) PETN.

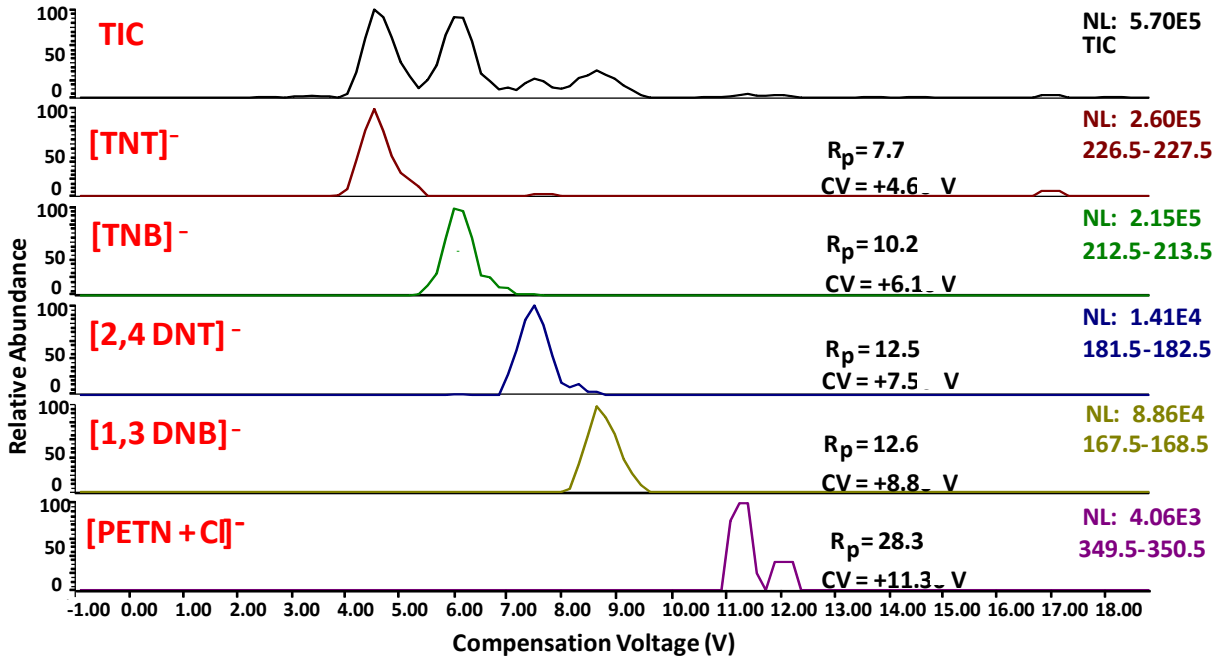

Figure 2-20. CV scan of a 2 ppm mixture of explosives on hemispherical cell at a DV -3214 V. (A) TIC, (B) TNT, (C) TNB, (D) 2,4-DNT, (E) 1,3-DNB, and (F) PETN.

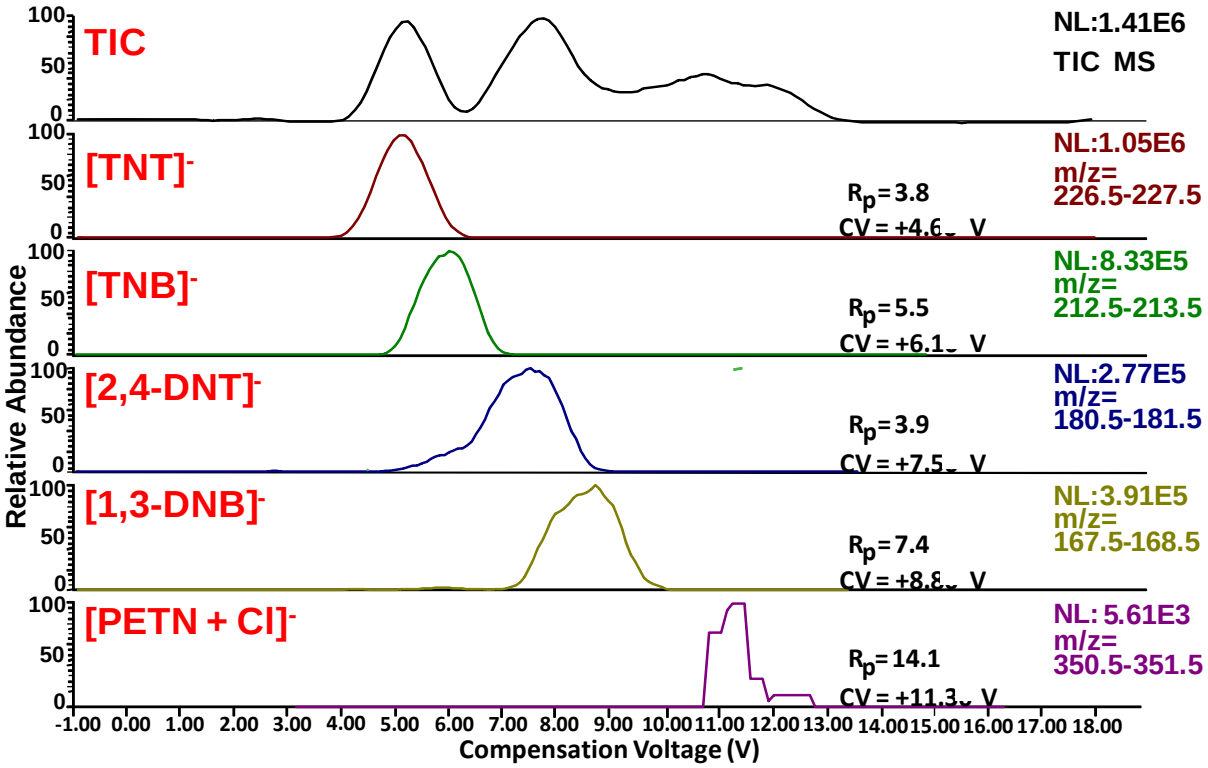

Figure 2-21. CV scan of a 2 ppm mixture of explosives on spherical cell at a DV -3214 V. (A) TIC, (B) TNT, (C) TNB, (D) 2,4-DNT, (E) 1,3-DNB, and (F) PETN.

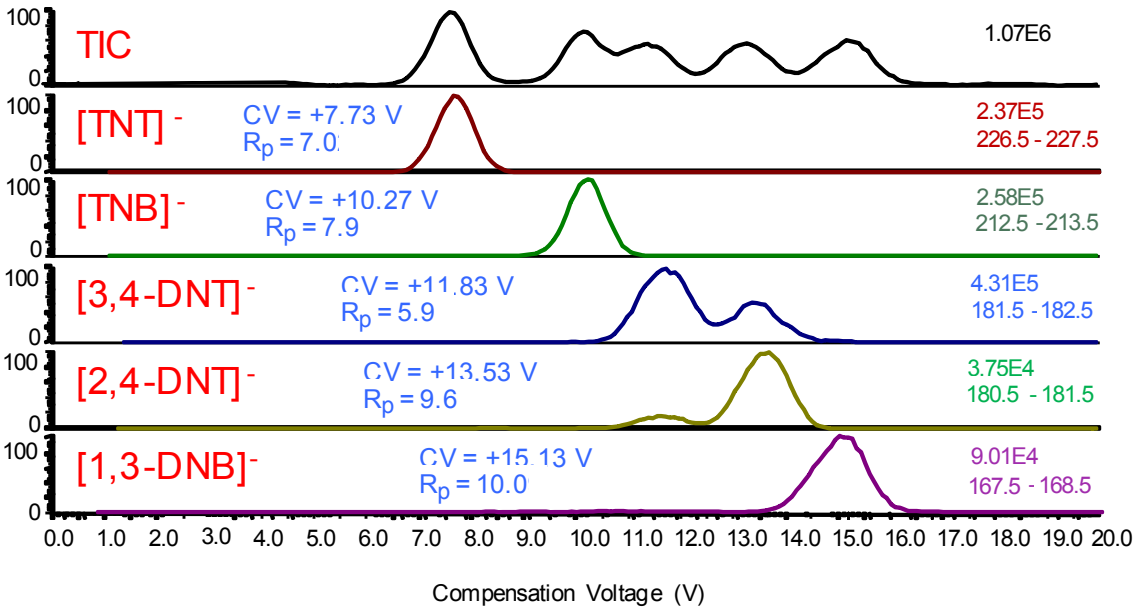

Figure 2-22. CV scan of a 2 ppm mixture of explosives on cylindrical cell at a DV -4700 (23,500 V/cm). (A) total ion current, (B) TNT, (C) TNB, (D) 3,4-DNT, (E) 2,4-DNT, and (F) 1,3-DNB.

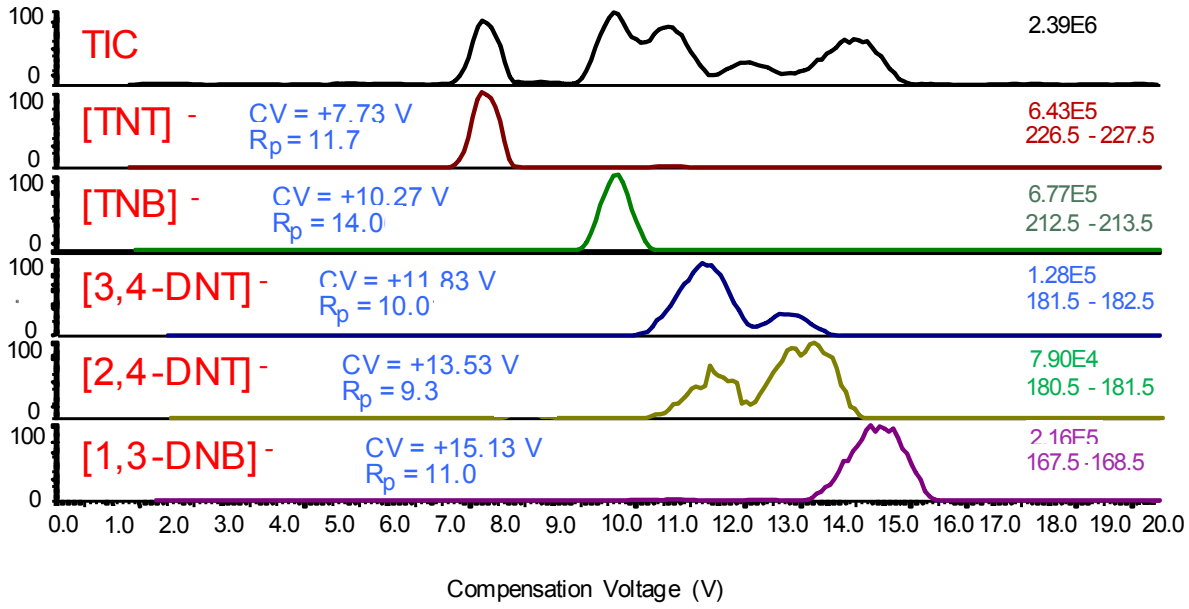

Figure 2.23. CV scan of a 2 ppm mixture of explosives on hemispherical cell at a DV -4700 V (23,500 V/cm). (A) total ion current, (B) TNT, (C) TNB, (D) 3,4-DNT, (E) 2,4-DNT, and (F) 1,3-DNB.

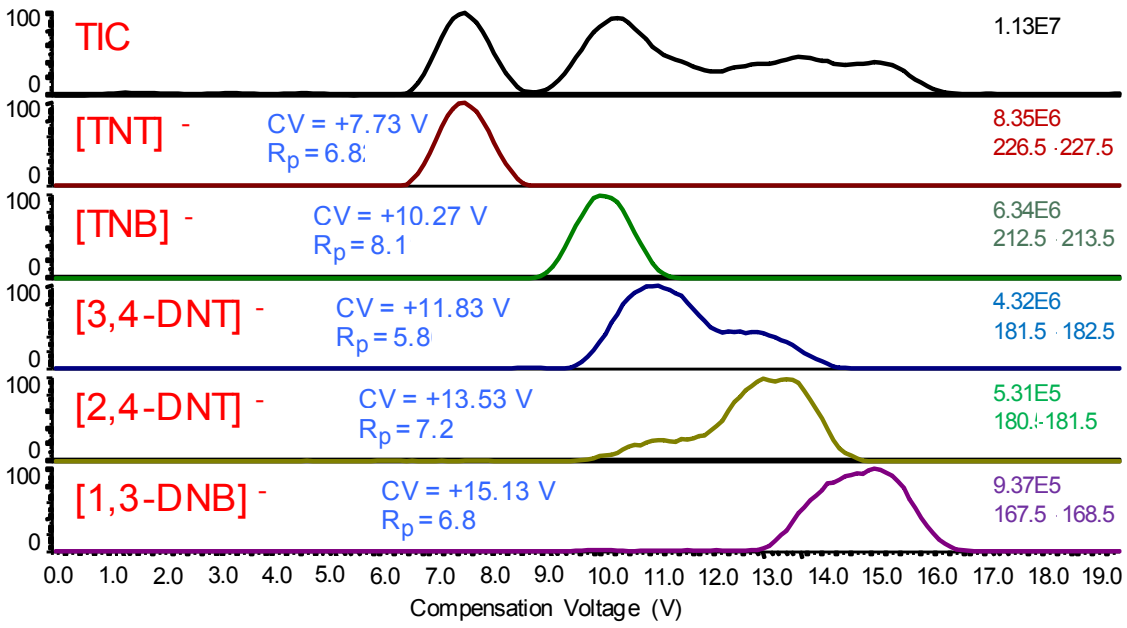

Figure 2-24. CV scan of a 2 ppm mixture of explosives on spherical cell at a DV -4700 V (23,500 V/cm). (A) total ion current, (B) TNT, (C) TNB, (D) 3,4-DNT, (E) 2,4-DNT, and (F) 1,3-DNB.

Table 2-1. Comparison of dimensions between Thermo-Fisher cylindrical and hemispherical cell.

	Hemispherical Cell	Thermo Fisher Cylindrical Cell
Distance from Curtain Plate to Outer Electrode	1.32 mm	2.20 mm
Curtain Plate Hole Diameter	2.00 mm	2.40 mm
Ion Inlet Diameter	1.50 mm	1.50 mm
Gap	2.00 mm	2.50 mm
Inner Electrode Radius	12.70 mm	6.50 mm
Outer Electrode Radius	14.73 mm	9.00 mm
Ion Outlet Diameter	1.00 mm	1.90 mm

Table 2-2. Comparison of dimensions between all three cells.

	Spherical Cell	Hemispherical Cell	Thermo Fisher Cylindrical Cell
Distance from Curtain Plate to Outer Electrode	1.32 mm	1.32 mm	2.20 mm
Curtain Plate Hole Diameter	2.00 mm	2.00 mm	2.40 mm
Ion Inlet Diameter	1.50 mm	1.50 mm	1.50 mm
Gap	2.00 mm	2.00 mm	2.50 mm
Inner Electrode Radius	12.70 mm	12.70 mm	6.50 mm
Outer Electrode Radius	14.73 mm	14.73 mm	9.00 mm
Ion Outlet Diameter	1.00 mm	1.00 mm	1.90 mm

Table 2-3. Anticipated ions and adducts for nitramine and nitrate ester explosives.

			APCI
Name	Mode	MW	Characteristic Ions (*m/z*)
RDX+Cl	negative	257	257 $[M+^{35}Cl]^-$, 259 $[M+^{37}Cl]^-$, 479 $[2M+^{35}Cl]^-$, 481 $[2M+^{37}Cl]^-$, 210 $[M+^{35}Cl\text{-}NO_2\text{-}H]^-$, 212 $[M+^{37}Cl\text{-}NO_2\text{-}H]^-$
HMX+Cl	negative	331	331 $[M+^{35}Cl]^-$, 333 $[M+^{37}Cl]^-$, 358 $[M+NO_3]^-$, 284 $[M+^{35}Cl\text{-}HNO_3]^-$, 286 $[M+^{37}Cl\text{-}HNO^3]^-$
NG+Cl	negative	227	262 $[M+^{35}Cl]^-$, 264 $[M+^{37}Cl]^-$, 289 $[M+NO_3]^-$, 489 $[2M+^{35}Cl]^-$, 491 $[2M+^{37}Cl]^-$
PETN+Cl	negative	351	351 $[M+^{35}Cl]^-$, 353 $[M+^{37}Cl]^-$

Table 2-4. Comparison of intensity values for RDX, HMX, NG, 2,4-DNT, PETN, TNT, and TNB between the Ionalytics cylindrical, hemispherical, and spherical FAIMS cell.

Explosive	Intensity of Cylindrical Cell	Intensity of Hemispherical Cell	Increase over Cylindrical	Intensity of Spherical Cell	Increase over Cylindrical
RDX	$7.55 \times 10^3 \pm S_E$ 38	$1.96 \times 10^4 \pm S_E$ 290	>2.6x	$7.25 \times 10^4 \pm S_E$ 405	~10x
HMX	ND	ND	0	ND	ND
NG	ND	ND	0	ND	ND
2,4-DNT	$4.23 \times 10^4 \pm S_E$ 200	$2.01 \times 10^5 \pm S_E$ 1763	4.8x	$7.27 \times 10^5 \pm S_E$ 3180	17x
PETN	$9.77 \times 10^3 \pm S_E$ 26	$5.28 \times 10^4 \pm S_E$ 750	5.5x	$1.03 \times 10^5 \pm S_E$ 2577	11x
TNT	$3.52 \times 10^4 \pm S_E$ 264	$2.90 \times 10^5 \pm S_E$ 2027	8.2x	$7.99 \times 10^5 \pm S_E$ 1856	23x
TNB	$5.63 \times 10^4 \pm S_E$ 218	$1.64 \times 10^5 \pm S_E$ 2081	~3.0x	$7.50 \times 10^5 \pm S_E$ 1201	>13x

Table 2-5. Comparison of CV, intensity, and resolving power between the Thermo-Fisher cylindrical at 16,000 V/cm and both the hemispherical and spherical FAIMS cell at 16,072 V/cm.

	Cylindrical Cell			Hemispherical Cell			Spherical Cell		
	CV Value (V)	Intensity	Resolving Power	CV Value (V)	Intensity	Resolving Power	CV Value (V)	Intensity	Resolving Power
TNT	+4.60 V	$1.01 \times 10^5 \pm S_E$ 333	2.80	+4.60 V	$2.60 \times 10^5 \pm S_E$ 333	7.70	+4.60 V	$1.06 \times 10^6 \pm S_E$ 5773	3.80
TNB	+6.10 V	$1.26 \times 10^5 \pm S_E$ 667	3.20	+6.10 V	$2.15 \times 10^5 \pm S_E$ 882	10.20	+6.10 V	$8.33 \times 10^5 \pm S_E$ 882	5.50
2,4-DNT	+7.50 V	$6.57 \times 10^3 \pm S_E$ 6	2.70	+7.50 V	$1.42 \times 10^4 \pm S_E$ 33	12.50	+7.50 V	$2.77 \times 10^5 \pm S_E$ 333	3.90
1,3-DNB	+8.80 V	$5.91 \times 10^4 \pm S_E$ 33	3.90	+8.80 V	$8.88 \times 10^4 \pm S_E$ 88	12.60	+8.80 V	$3.91 \times 10^5 \pm S_E$ 333	7.40
PETN	ND	0	0.00	+11.30 V	$4.04 \times 10^3 \pm S_E$ 15	28.30	+11.30 V	$5.63 \times 10^3 \pm S_E$ 9	14.10

Table 2-6. Comparison of resolution between the Thermo-Fisher cylindrical cell at 16,000 V/cm and both the hemispherical and spherical FAIMS cell at 16,072 V/cm.

	Cylindrical Cell	Hemispherical Cell	Spherical Cell
Rs between TNT and TNB	0.55	0.97	0.75
Rs between TNB and 2,4-DNT	0.45	1.03	0.61
Rs between 2,4-DNT and 1,3-DNB	0.31	1.08	0.51
Rs between 1,3-DNB and PETN	ND	2.17	1.56

Table 2-7. Comparison of CV, intensity, and resolving power between the Ionalytics cylindrical, hemispherical, and spherical FAIMS cell at 23,500 V/cm.

	Cylindrical Cell			Hemispherical Cell			Spherical Cell		
	CV Value (V)	Intensity	Resolving Power	CV Value (V)	Intensity	Resolving Power	CV Value (V)	Intensity	Resolving Power
TNT	+7.73 V	$2.37 \times 10^5 \pm S_E$ 333	7.02	+7.73 V	$6.41 \times 10^5 \pm S_E$ 333	11.73	+7.73 V	$8.34 \times 10^6 \pm S_E$ 12018	6.82
TNB	+10.27 V	$2.59 \times 10^5 \pm S_E$ 667	7.90	+10.27 V	$6.76 \times 10^5 \pm S_E$ 667	14.06	+10.27 V	$6.32 \times 10^6 \pm S_E$ 8819	8.11
3,4-DNT	+11.33 V	$4.32 \times 10^4 \pm S_E$ 88	5.92	+11.33 V	$1.24 \times 10^5 \pm S_E$ 185	10.01	+11.33 V	$4.30 \times 10^6 \pm S_E$ 8819	5.86
2,4-DNT	+13.53 V	$3.74 \times 10^4 \pm S_E$ 58	9.66	+13.53 V	$7.89 \times 10^4 \pm S_E$ 88	9.38	+13.53 V	$5.31 \times 10^5 \pm S_E$ 1453	7.28
1,3-DNB	+15.13 V	$9.01 \times 10^4 \pm S_E$ 58	10.09	+15.13 V	$2.16 \times 10^5 \pm S_E$ 333	11.00	+15.13 V	$9.34 \times 10^5 \pm S_E$ 1527	6.88

Table 2-8. Comparison of resolution and peak width between the Thermo-Fisher cylindrical, hemispherical and spherical FAIMS cell at 23,500 V/cm.

	Cylindrical Cell	Hemispherical Cell	Spherical Cell
Rs between TNT and TNB	1.65	2.33	1.27
Rs between TNB and 3,4-DNT	0.51	0.47	0.33
Rs between 3,4-DNT and 2,4-DNT	0.57	0.57	0.50
Rs between 2,4-DNT and 1,3-DNB	0.69	0.67	0.42

Table 2-9. Repeatability of CV values on the spherical cell from five replicate runs for TNT.

TNT	DV (V)	-705	-1099	-1410	-1706	-2000	-2394	-2690	-2820	-3018	-3378
	CV (V)	0.3	0.4	0.7	0.9	1.5	2.4	3.3	3.8	4.3	5.0
	SD	0.04	0.02	0.02	0.005	0	0.009	0	0	0.01	0
	RSD%	2.3	1.4	1.2	0.2	0	0.5	0	0	0.8	0

Table 2-10. Linear dynamic range and limit of detection for TNT collected by full-scan and SIM mode.

	Full Scan			SIM		
			LOD			LOD
	Linear Dynamic Range (ng/mL)	Corr. Coef. (R^2)	Concn. (ng/mL)	Linear Dynamic Range (ng/mL)	Corr. Coef. (R^2)	Concn. (ng/mL)
TNT	16 - 10000	0.9951	4	3 - 10000	0.9968	1

CHAPTER 3
EVALUATION OF FAIMS WAVEFORMS APPROACHES

Introduction

High-field asymmetric ion mobility spectrometry, or FAIMS, is an emerging detection technology which can operate at atmospheric pressure to separate gas-phase ions as first described in detail by Buryakov, *et al*.[20] FAIMS is similar to conventional ion mobility spectrometry (IMS), which utilizes relatively low electric fields to propel ions through a drift gas chamber and separate these ions according to their drift velocity. IMS, is an important technique for the detection of many compounds, including narcotics, explosives, and chemical warfare agents because of its high sensitivity and amenability to miniaturization for field-portable applications.[26] In IMS, the ion drift velocity is proportional to the field strength at low electric fields (~200 V/cm) and thus an ion's mobility (K) is independent of the applied field. At high fields (~10,000 V/cm), however, ion mobilities become dependent on the applied field and are better represented by K_h (equation 1-6), a non-constant high-field mobility term. Variations in K_h from the low-field K, and the compound-dependence of that variation affords FAIMS its separation power. FAIMS utilizes a combination of alternating current (AC) and direct current (DC) voltages to transmit ions of interest and filter out other ions, thus improving signal to noise ratio. FAIMS can also help reduce false positives, since two different compounds having the same low-field mobility can often be distinguished in a high-field environment.[61]

Ions are separated in FAIMS by their difference in mobility at high (K_h) and at low (K) electric fields. At a constant gas number density, N, the non-linear dependence of an ion's mobility in high electric fields is given by equation 1-6 and is re-shown here

$$K_h(E) = K_0\left[1 + \alpha\left(\frac{E}{N}\right)^2 + \beta\left(\frac{E}{N}\right)^4 + \ldots\right] \quad (1\text{-}6)$$

where K_0 is the ion mobility coefficient at zero electric field and α and β describe the dependence of the ion's mobility at a high electric field in a particular drift gas.[40] This equation is an infinite series, but at realistic field intensities the terms above the 4th order become insignificant.[41, 42] In FAIMS, one of the electrodes is typically held at a ground potential while the other has an asymmetric waveform applied to it. The most commonly used asymmetric waveform, described by $V(t)$ in equation 3-2, consists of a high-voltage component (also referred to as V_1 or dispersion voltage [DV]) which lasts for a short period of time (t_1) relative to a longer lasting (t_2) low-voltage component (V_2) of opposite polarity. Most FAIMS work up to date has employed a sinusoidal wave, plus its first harmonic at twice the frequency, as shown in equation 3-2, where ω is the frequency in radians per second. The waveform is constructed so that the voltage-time product applied to the electrode is equal to zero as displayed in equation 1-7.

$$V(t) = (0.61)V_1\, sin(\omega t) + (0.39)V_1 \sin\left(2\,\omega t - \frac{\pi}{2}\right) \ldots \quad (3\text{-}2)$$

At high electric fields, the application of this waveform will cause an ion to experience a net drift toward one of the electrodes. Ions passing between the electrodes encounter this displacement because the ion's mobility during the high-voltage component (K_h) is different than that from the low-voltage mobility (K). In other words, the ion will move a different distance during the high-voltage portion than during the low-voltage portion. This ion will continue to migrate towards one of the electrodes and subsequently be lost unless a DC compensation voltage (CV) is applied to offset the drift. The CV values required to offset the drift of different ions will be different if the K_h/K ratio of the ions are different. Thus, a mixture of compounds can be successfully

separated by scanning the CV, allowing each compound to transmit at its characteristic CV, creating a CV spectrum.

When higher electric fields are applied to the FAIMS electrodes, an ion can have three possible changes in ion mobility. The mobility of type A ions increases with increasing electric field strength, the mobility of type C ions decreases, and the mobility of type B ions increases initially before decreasing at yet higher fields.[43, 61] Most low-mass ions (< *m/z* 300) are type A ions, whereas most high-mass ions are type C ions.[62]

Sum of Sines Waveform

The dependence of an ion's mobility in a time-varying electric field makes the design of the waveform in FAIMS an essential feature for its overall performance. [63] As mentioned above, most FAIMS work to date has employed a sinusoidal wave plus its first harmonic at twice the frequency, as described in equation 3-2. If the amplitude and CV are being applied to the same electrode, then the addition of CV should be included in equation 3-2. Equation 3-2 results in an asymmetric waveform of the type shown in figure 3-1a. The shape of the waveform is a parameter that contributes to the value of the experimentally measured (compound-dependent) CV for transmission of an ion. A symmetrical waveform (sine or square) should result in CV = 0 V for transmission of all types of ions. Asymmetry of the waveform is required for ion separation and is expressed by differences in the CV.[43]

Square Waveform

Even though most FAIMS experiments have made use of the sum-of-sines waveform, theoretical studies have suggested that a rectangular waveform (as shown in figure 3-1b) would be ideal for FAIMS analyses.[63-65] Analytical considerations show that rectangular waveforms may improve ion separation efficiency, resolution and/or

sensitivity as compared to sinusoidal waveforms.[62, 65-67] Unfortunately, the excessive power load imposed by high frequency, high voltage pulses with steep rise times has hindered the development of electronics that deliver rectangular pulses for driving separations based on differential ion mobility.[63]

Intuitively, the use of an asymmetric square waveform for FAIMS would seem to maximize the differences during the high and low field portions of the electric field. These high to low periods of the waveform permit an ion to experience a maximum of unequal voltages maximizing the CV. In previous studies, there have been concerns that the time it takes an ion to respond to the idealized asymmetric square waveform and reach "steady state," or terminal, drift velocity might be sufficiently long enough to introduce error due to the transient electric field.[42] Lin *et al.* showed that, to the first order, this can be neglected if the time for reaching terminal velocity is small relative to the total drift time. Since the estimated time necessary to reach this velocity in a transient electric field is in the picosecond range and the drift time is in the millisecond range, this factor can be ignored.

Because FAIMS has continuous ion separation capabilities, it is attractive to use in conjunction with a mass spectrometer. This union was utilized to offer orthogonal detection methods, one separating ions according to their mobilities through a gas and the other separating ions according to their mass-to-charge ratios. In this chapter we describe how the independent control (frequency, amplitude, and duty cycle) of a square waveform can help to more completely characterize FAIMS in terms of transmission, resolution, and separation in comparison to a sum-of-sines waveform. Previous experiments have shown the duty cycle to have a strong influence on ion

separation with planar electrodes.[63] Here, the duty cycle is defined as the ratio of the width of the high-voltage pulse to waveform period. A miniature FAIMS cell powered by a digitally driven circuit producing a square waveform will be described in comparison to an analog sum-of-sines waveform. A full comparison of separation and sensitivity is performed over the overlapping range provided by the waveform generators. This chapter also includes SIMION 8[68] modeling to help validate experimental results.

Experimental

The traditional sinusoidal waveform was created by an Ionalytics GPI 1000 FAIMS system alpha prototype waveform generator which only runs with a 2:1 ratio (33% duty cycle) at a frequency of 750 kHz. This waveform was applied to one of the plates and a reference lead to the other plate. Each individual component waveform was capacitance tuned for the electrodes and added together to produce a waveform similar to the one shown in figure 3-1a. The full range of operation for the Ionalytics alpha prototype is (+/-) 300 V to (+/-) 4000 V; the range utilized for this research was from (+/-) 300 V to (+/-) 800 V, since higher voltages could arc within the short distances of the cell. Data were processed using the mass spectrometer instrument software (described below).

The square waveform generator used in these studies was constructed by Implant Sciences Corporation; a schematic is shown in figure 3-2. In this computer-generated waveform, three of the four variables (V_1, V_2, t_1, and t_2) are specified; the fourth is deduced from the balanced equation 1-7. The waveform generator is the subject of a patent application.

The frequency, duty cycle, and amplitude on the square waveform are all independently controlled. The square generator can provide positive DV values from

+50 V to +750 V. For this reason all experiments with the Ionalytics alpha prototype were only run with positive amplitude values. Three different frequencies (250, 333, 500 kHz) and six different duty cycles (25%, 30%, 33.3%, 35%, 40%, and 45%, defined as $t_1/(t_1 + t_2)$) were evaluated on this waveform generator unless otherwise noted. All experiments employed a CV separation over a 10 V range at a scan rate of 5 V/min. Data were processed using instrument software interface (DMS Interface Version 0.25) created by Implant Sciences.

The planar geometry FAIMS cell, as shown in figure 3-2a – c, was designed by the University of Florida Chemistry Department Machine Shop and consists of two parallel stainless steel plates (5 mm wide, 15 mm long, 1 mm thick) encased and recessed in a PEEK support (8mm wide, 18 mm long, 3 mm thick) that provides mechanical stability and electrical insulation. Electrical connections to the individual plates were made via posts spot welded to the plates through holes in the PEEK support. The gap within the FAIMS cell (0.38 mm) was maintained by fused silica capillaries as shown in the figure 3-2c . The top and bottom plates were then secured to each other through the PEEK with 4 screws to ensure mechanical stability and alignment.

The FAIMS cell was interfaced directly to the heated capillary inlet of an LCQ (Thermo Scientific) quadrupole ion trap mass spectrometer (QITMS) with the aid of a home-built end-cap connector piece. All experiments were performed utilizing this commercial bench-top MS. The end-cap piece was made of polyaryletheretherketone (PEEK) and is displayed in figure 3-2 (top left). End-cap piece and FAIMS cell were wrapped in Teflon to ensure no signal loss occurred between these connections. No

curtain plate or curtain gas was used and no attempt to perform additional ion desolvation was made. Conventional atmospheric pressure chemical ionization (APCI) was employed to produce gas phase ions. Nitrogen was used as the nebulizing (sheath) and auxiliary gases. APCI and heated capillary temperatures were held at 75 °C. Analyte samples were infused with a 500 µL Hamilton syringe at 15 µL/min. Solutions were injected directly via the syringe pump of the LCQ. Data acquisitions were performed using full scan mode (50-500 *m/z*) with a maximum injection time of 100 ms for automatic gain control (AGC). Data were processed using the instrument software interface (Xcalibur version 1.4 SR1).

In this chapter, a common explosive, 2,4,6-trinitrotoluene (TNT) was utilized. This explosive was provided by Dr. Jehuda Yinon of the Weizmann Institute of Science, and was obtained from the Analytical Laboratory of the Israeli Police Headquarters. Negative ion mode was employed with APCI. The explosive solution was diluted in a solvent mixture consisting of 65% methanol and 35% de-ionized water. Utilizing a combination of methanol and water as a solvent allows the use of lower vaporizer temperatures than water alone; the low vaporizer temperature help to avoid the degradation of fragile explosive analytes. In this research, all solutions were diluted to a concentration of 10 ppm unless otherwise noted.

SIMION 8, the ion trajectory modeling program[68], was utilized in an effort to optimize the performance of the miniature FAIMS cell and validate experimental results. The influences of pneumatic and electrostatic forces at atmospheric pressure are shown. The variables used in this investigation include gas flow, DV, CV, analytical gap (spacing between the plates), frequency of the asymmetric waveform, its shape

(sinusoidal versus square), and its duty cycle. The potential array of the FAIMS analyzer consisted of parallel plates (5 mm wide, 15 mm long, and separated by a gap, G = 0.5 mm). Statistical Diffusion Simulation[68] (SDS) user program was used to model the ion motion at atmospheric pressure. By modeling both diffusional and mobility terms of ions in a neutral gas, the effects of high pressure collisions are taken into account by the SDS user program. All simulations were performed using TNT, $[M]^-$, ions (*m/z* = 227) for which the low field and high field mobilities are known.[62, 69-71]

Results and Discussion

Influence of Dispersion Voltage on Compensation Voltage, Peak Width and Resolving Power

The characterization and performance of the square waveform on planar FAIMS ion separation was investigated. In FAIMS, ions are separated based on the change in their mobility at high vs. low electric fields. Thus, theoretically, the higher the field, the better separation that would be obtained. Generally, the magnitude of the CV increases as the DV increases for low mass ions (*m/z* usually below 300). This behavior is verified with both the sum-of-sines and square waveform generators, as displayed in figure 3-3a. The plot shows CV as a function of DV for both waveforms with the sine wave at 750 kHz and the square wave at three different frequencies (250, 333, and 500 kHz). The duty cycle for the sine waveform was 33% (not adjustable); a duty cycle of 25% was selected for the square waveform. It is evident that, for both square and sine waves, CV increases with DV, with square waveform giving higher CV magnitudes within the overlapped DV range (300-350 V). The frequency of the square waveform has no significant effect on the CV. Further insight into the behavior of the [M]- ion in the planar geometry FAIMS cell can be gained by simulation of ion trajectories with

SIMION. Figure 3-4 compares the plots for CV vs. DV for both waveforms, over a wider range of DV that can be achieved with our current electronics. Comparing these plots with the experimental data in figure 3-3a shows the same trend of higher CV values for square wave than for sine wave at the same DV (although only a 1.5x increase, less than the 2.5x increase observed experimentally). Note that the simulated CV values are generally smaller than those observed experimentally, perhaps because of the increased CV values recently observed in the presence of solvent vapor in the FAIMS cell.[72]

In a planar geometry FAIMS cell, ions are presumably distributed evenly across the gap between the two electrodes. There is typically better resolution with this geometry with an uniform electric field than with the focusing effect observed with curved electrodes.[73] Peak shapes, as well as transmission, are affected by lateral diffusion and space charging (also known as ion-ion repulsions). Figure 3-3b shows that experimental peak widths (full width at half maximum, FWHM) generally increase as DV increases for both waveforms, although the peak width for the square wave increases only slightly over the available DV range. The dramatic increase in peak width for the square waveforms around DV 150 V is due to splitting of the main TNT peak into two peaks. Peak splitting is shown in figure 3-5. The figure displays three CV scans of the extracted chromatograms of *m/z* 227. The CV scan is from -2 to 8 V over two minutes (5 V/min). The frequency and duty cycle applied were 250 kHz and 25%, respectively. The figure shows a progressive splitting of the CV peak of mass 227 as the dispersion voltage is increased (3-5a - 3-5f). It was suspected that this ion, with identical mass (*m/z* 227), is not TNT and therefore has a different compensation

voltage. As the electric field increases within the gap of the FAIMS cell the difference in their mobility becomes more apparent. Figure 3-5 is a great example of how FAIMS can be utilized as an orthogonal detection method when applied to MS.

Resolving power ($R_{p\,FAIMS}$) indicates the ability of the FAIMS cell to resolve a peak at a particular compensation voltage.[74] $R_{p\,FAIMS}$ is defined as the CV divided by the peak width at FWHM and I, as shown in equation 2-6. Figure 3-3c displays that the $R_{p\,FAIMS}$ increases with DV for both waveforms, although at any given DV, higher $R_{p\,FAIMS}$ values are obtained for the square waveform. Even though broader peaks are observed at higher dispersion voltages, as shown in figure 3-3b, the even greater increase in CV (figure 3-3a) results in enhanced $R_{p\,FAIMS}$.[75]

Influence of Frequency on Compensation Voltage, Peak Width, and Resolving Power

The rectangular asymmetric waveforms were monitored at different amplitudes and frequencies with a 100 MHz Tektronix TDS 1012B oscilloscope, as shown in figure 3-6. The requested values of the width, t_1, and the amplitude, V_1, of the high voltage pulse are indicated on the figure. It should be noted that the traces are offset vertically from the 250 kHz trace for ease of visualization. All the traces displayed in figure 3-6 are at 25% duty cycle. Here, the duty cycle, d, is defined as

$$d = \frac{t_1}{(t_1+t_2)} \tag{3-3}$$

Figure 3-3 shows that the frequency of the waveforms has little effect on CV, PWHM, or $R_{p\,FAIMS}$. This is as expected, since the frequency of the waveform (and thus the rate of ion oscillations perpendicular to the gas flow) should not affect the CV where the ion is transmitted.

While the duty cycle of the sine waveform is not variable, it is quite simple to vary the duty cycle of the square waveform. At lower duty cycles (where the waveform deviates more from symmetrical) $R_{p\,FAIMS}$ increases, as displayed in figure 3-9. Note that at DV values between100 and 200 V, a 25% duty cycle yields an $R_{p\,FAIMS}$ ~5x higher than a 45% duty cycle.

Influence of Frequency on Sensitivity

Higher frequencies are generally thought to improve ion separation at the expense of transmission.[65] The loss of transmission can be better tolerated by increasing the frequency, which however is limited by the electronics and creates more distortion in the rectangular shape of the waveform. Figure 3-10 displays the effect of frequency on sensitivity (3-10a) and peak area (3-10b) as a function of dispersion voltage. It is known that a reduction of the ion oscillation amplitude is due to the increased frequencies. This increased frequency helps to intensify the transmission of the specified ion and this is verified in figure 3-10. It should be noted that a 25% duty cycle was selected for these graphs to be able to show 500 kHz frequency data. Higher cycles displayed the same behavior.

Influence of Duty Cycle on Sensitivity

The duty cycle is one FAIMS parameter that has not been explored in the past since the duty cycle of the sine waveform (used in all commercial FAIMS systems) is fixed to 33%. In this work, the effect of duty cycle of the square waveform on sensitivity has been explored by holding the frequency at a fixed value of 250 kHz and 333 kHz. The results shown in figure 3-11 indicate that the signal intensity increases as the duty cycle decreases. Indeed, decreasing duty cycle from 45% to 25% increases the signal

by a factor of 2 to 3. Lower duty cycles give greater sensitivity at all frequencies examined.

Lower Concentration Experiments

To evaluate whether the performance of square wave planar FAIMS is a function of concentration, samples varying over a 100x concentration range were evaluated; the results (CV, PWHM, R_p, and signal intensity) are displayed in table 3-1. These data verify that the reproducibility of CV peak positions and R_p are unaffected by concentration within experimental error. Note as well that signal intensity varies linearly with concentration over two decades.

Conclusions

This paper demonstrated for the first time the practical implementation and characterization of square wave FAIMS on a miniature planar system. The independent control of frequency, amplitude, and duty cycle of a computer-generated square waveform can provide in a more complete characterization of FAIMS in terms of transmission, resolution, and separation compared to a sum of sines waveform. Square wave FAIMS delivers better separation and resolving power, as predicted with ion trajectory simulation. The increase of frequency was shown to increase sensitivity but had little effect on CV, peak width, and R_p. The lower the duty cycle the higher our peak area and signal intensity. Duty cycle decreases from 45% to 25% also showed a 5x increase in R_p . Comparison of results with the sum of sines waveform shows that the square waveform can provide better separation and resolving power, albeit at some cost in transmission and thus sensitivity. Further studies should be performed to compare square and sine waveforms with additional explosives and mixture of explosives. It would also be interesting to compare the two waveforms with different cell

dimensions and with different cell geometries. The major limitation of the square waveform is the limited voltage and power that can be obtained with practical waveform generators.

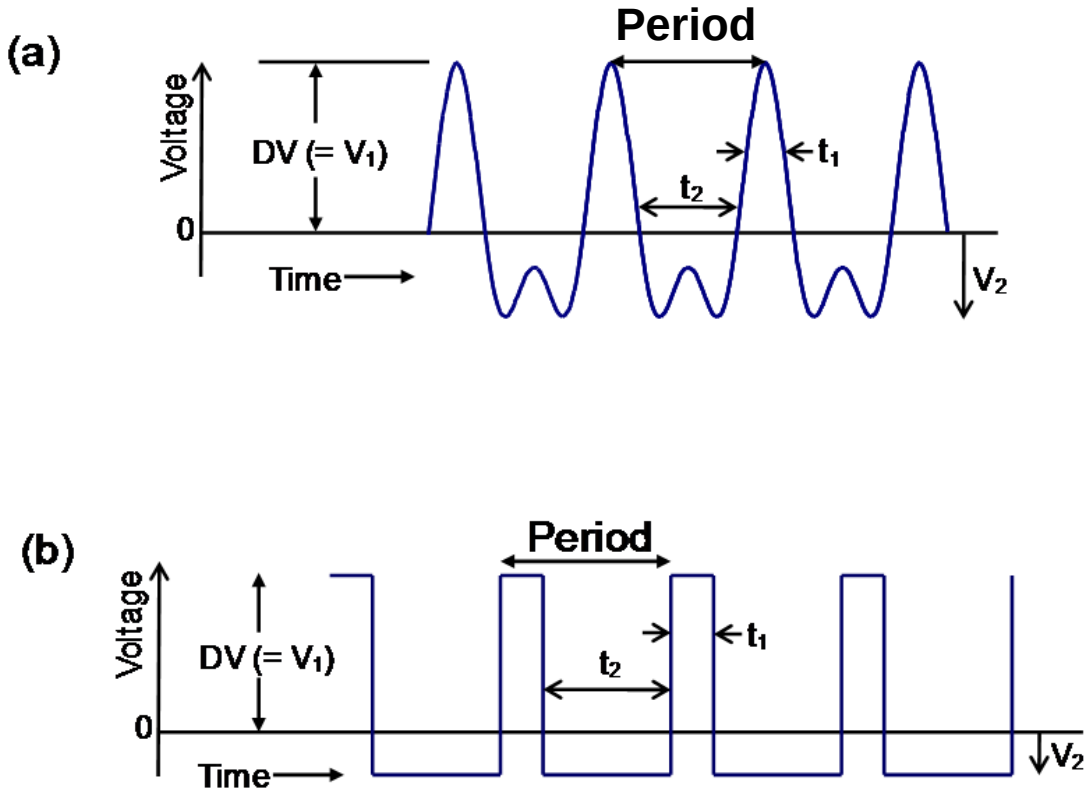

Figure 3-1. Schematic of **(a)** an asymmetric sum-of-sines waveform and **(b)** a rectangular waveform.

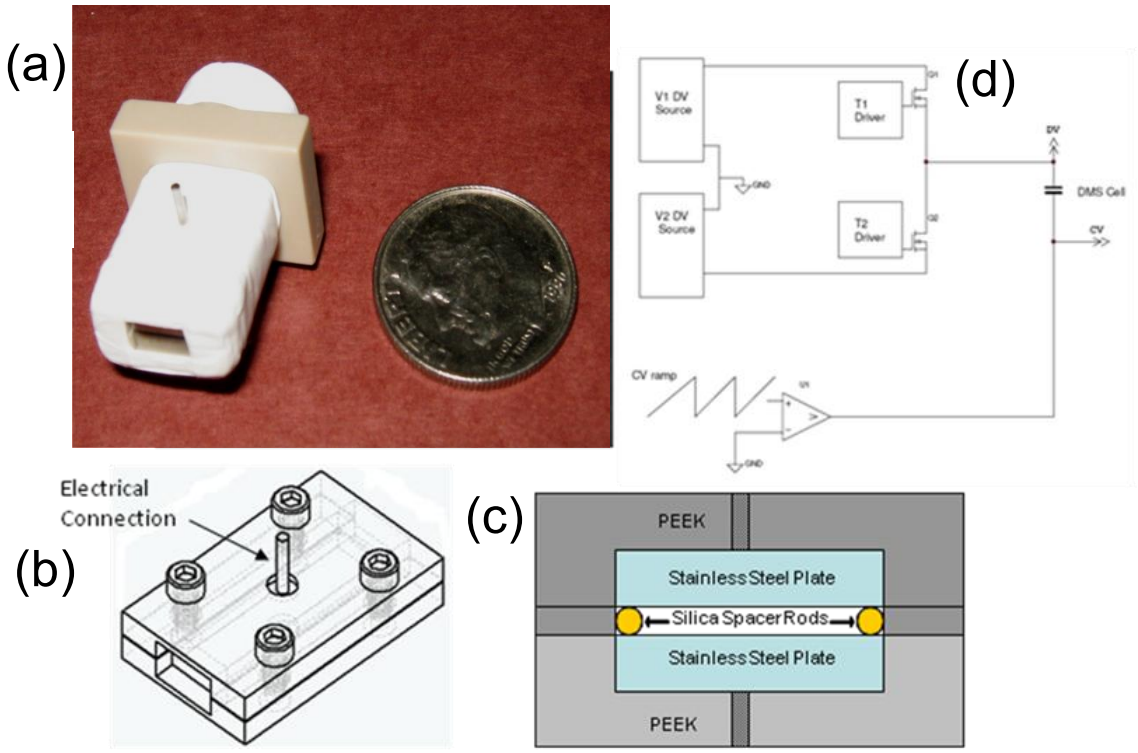

Figure 3-2. Photograph **(a)**, perspective and cross-sectional views **(b and c)** of miniature planar FAIMS cell. Square wave generator circuit diagram is also shown **(d)**.

(a)

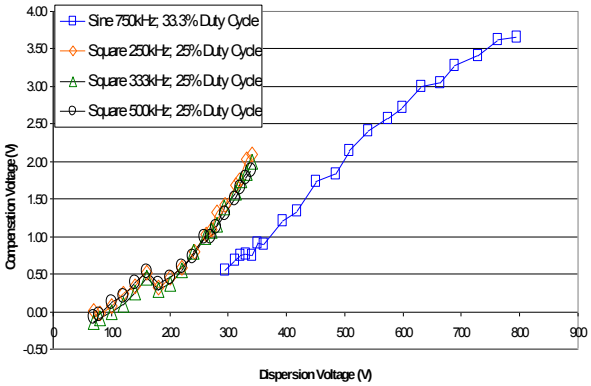

(b)

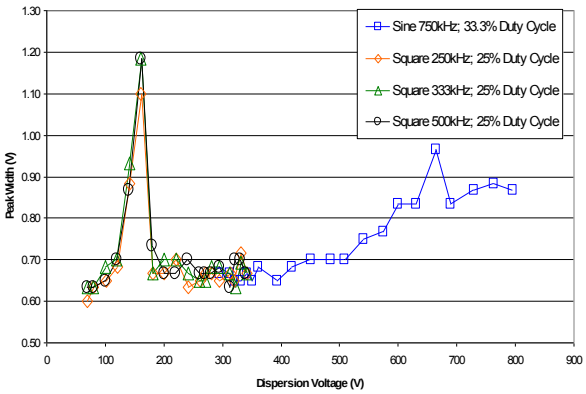

(c)

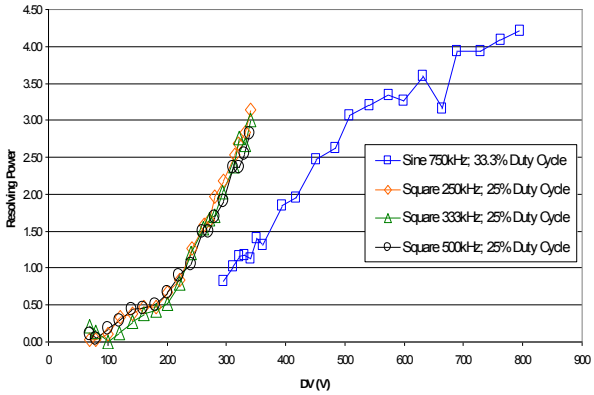

Figure 3-3. Graphs displaying behavior of CV **(a)**, peak width **(b)**, and resolving power **(c)** as a function of DV.

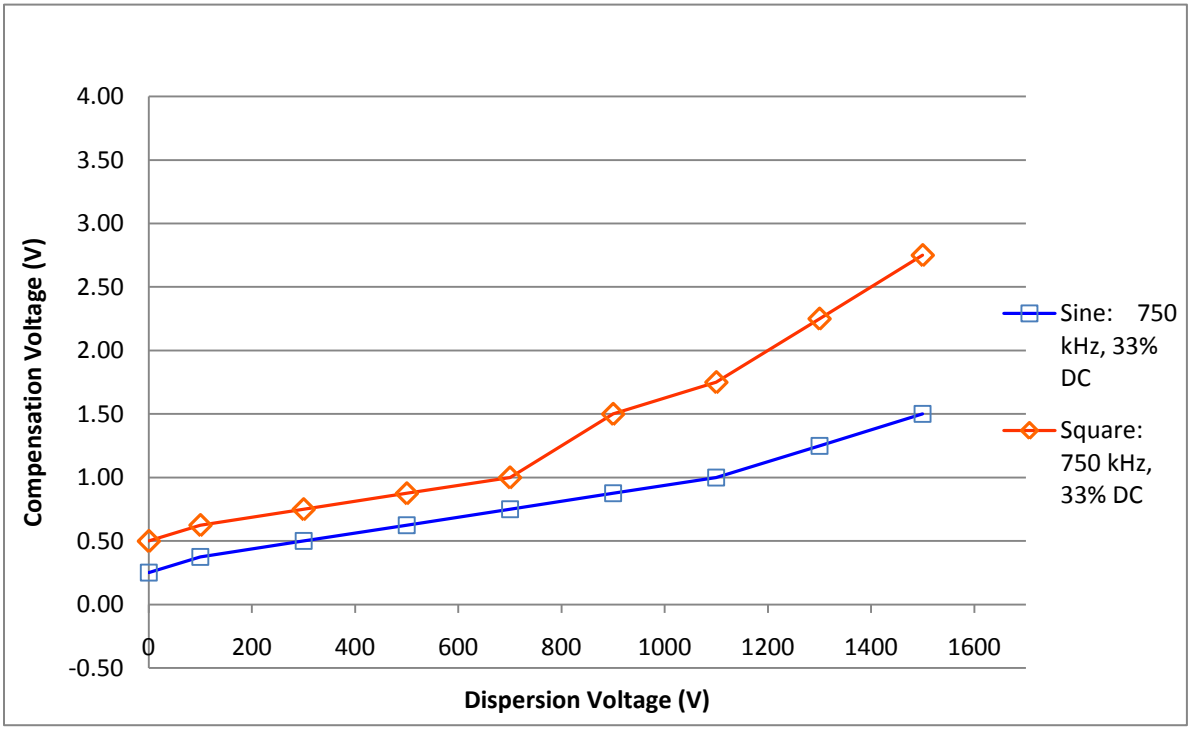

Figure 3-4. CV versus DV simulation data for the $[M]^-$ ion of TNT.

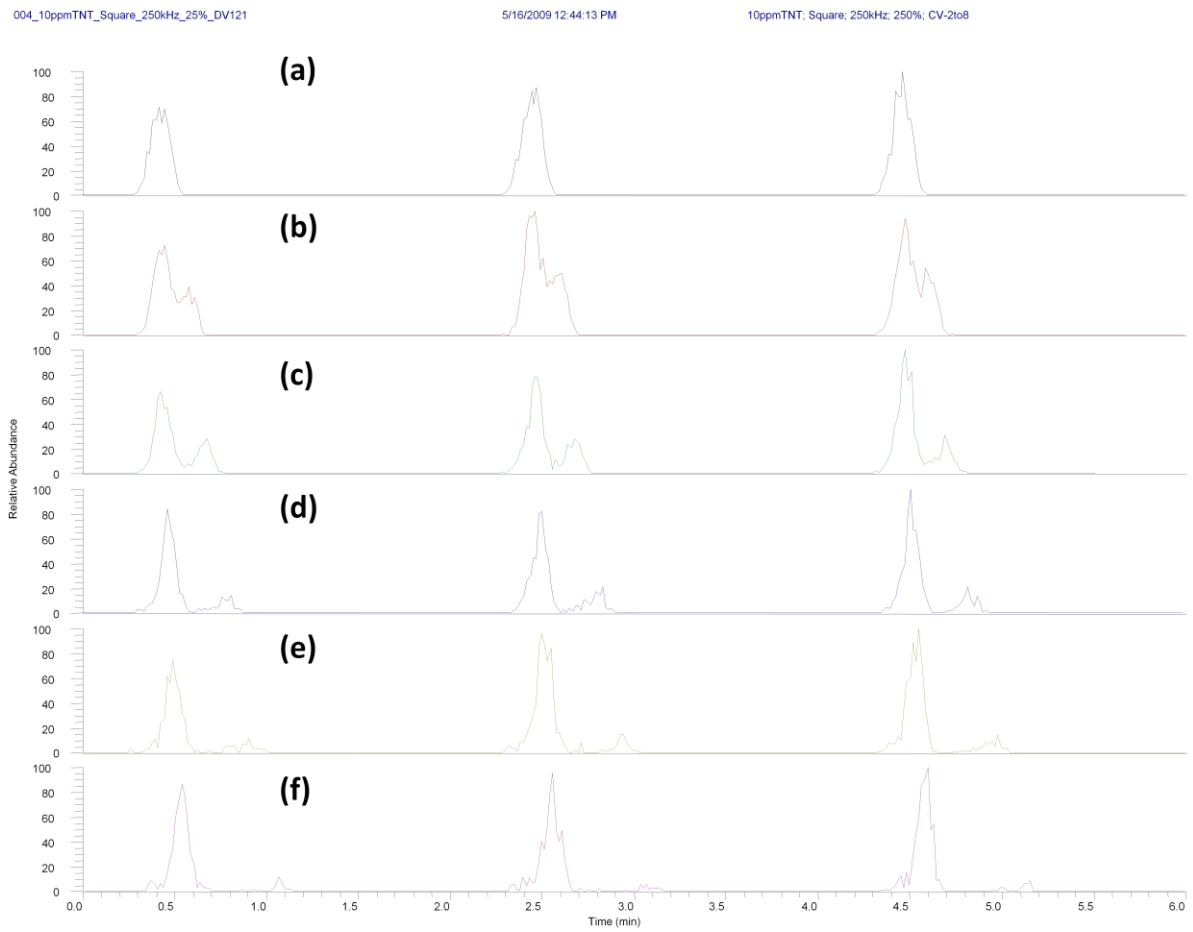

Figure 3-5. Three CV scans of 10 ppm TNT. Peak splitting is observed as DV is increased from **(a)** to **(f)**. **(a)** is a DV +121 V, **(b)** +161 V, **(c)** +181 V, **(d)** +201 V, **(e)** +221 V, and **(f)** +242 V.

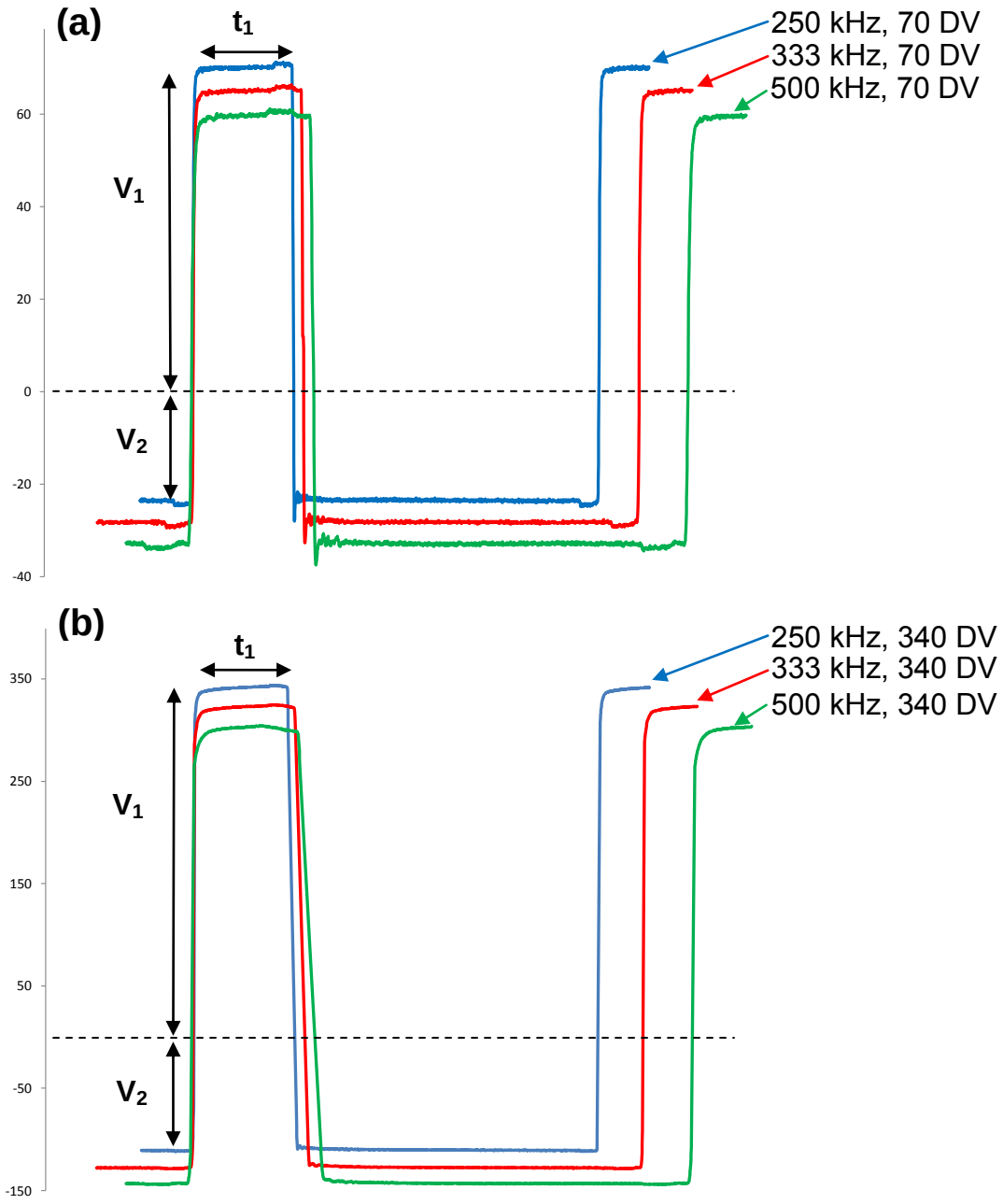

Figure 3-6. Scope traces of square waveforms at different frequencies for amplitudes **(a)** DV 70 and **(b)** DV 340 where V_1 is the amplitude (DV) and t_1 is the width of the high voltage pulse. Waveforms are offset for ease of visualization.

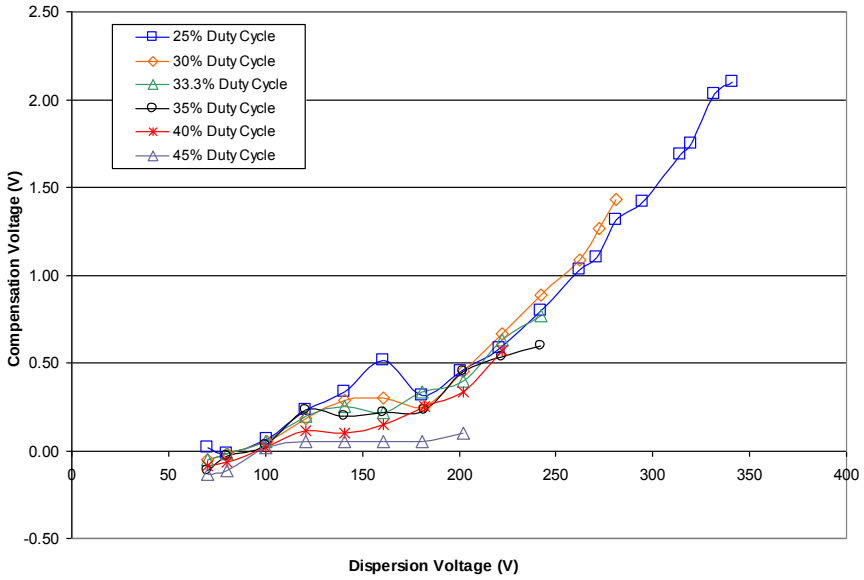

Figure 3-7. Graph displaying CV as a function of DV. For 250 kHz the duty cycle is shown to have little effect.

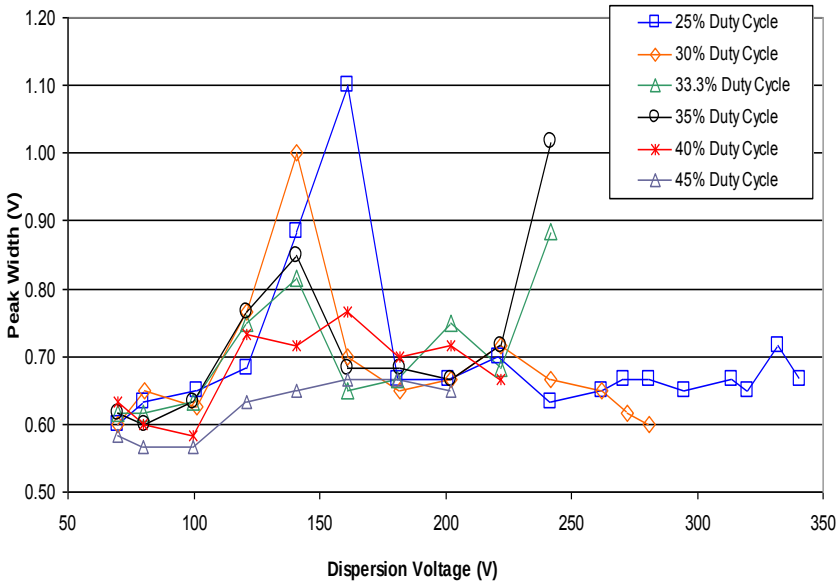

Figure 3-8. Graph displaying peak width as a function of dispersion voltage. For 250 kHz the duty cycle is shown to have no effect.

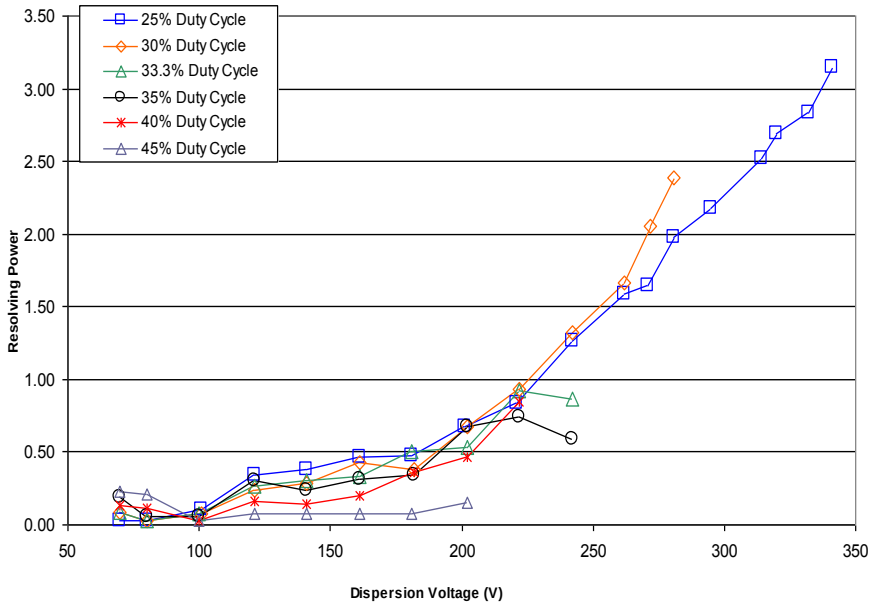

Figure 3-9. $R_{p\,FAIMS}$ as a function of DV at six different duty cycles.

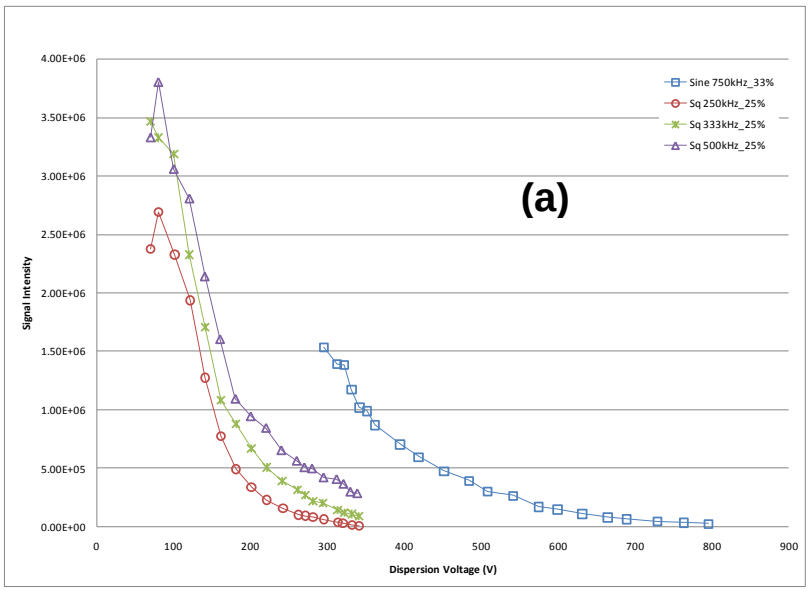

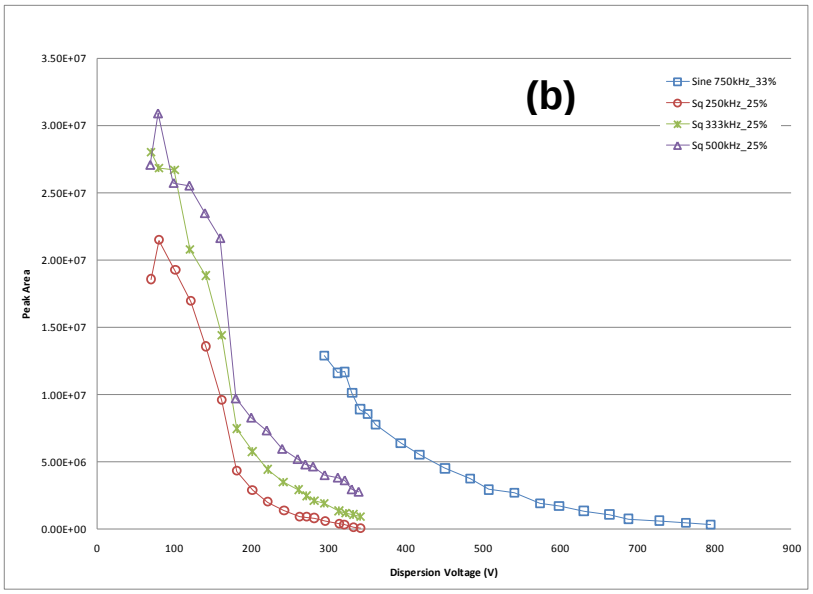

Figure 3-10. Graphs displaying effect of square wave frequency on sensitivity **(a)** and peak area **(b)**.

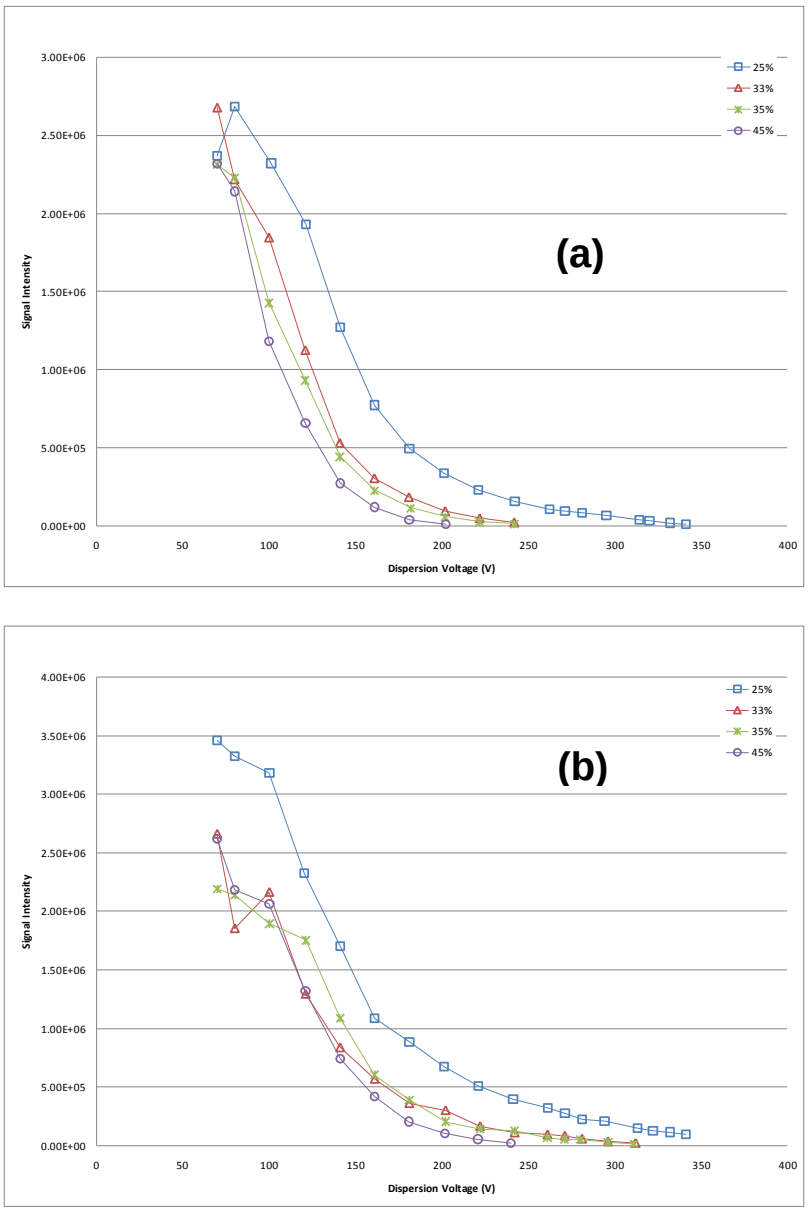

Figure 3-11. Graphs displaying the effect of duty cycle on sensitivity. Frequency is fixed to 250 kHz **(a)** and 333 kHz **(b)**.

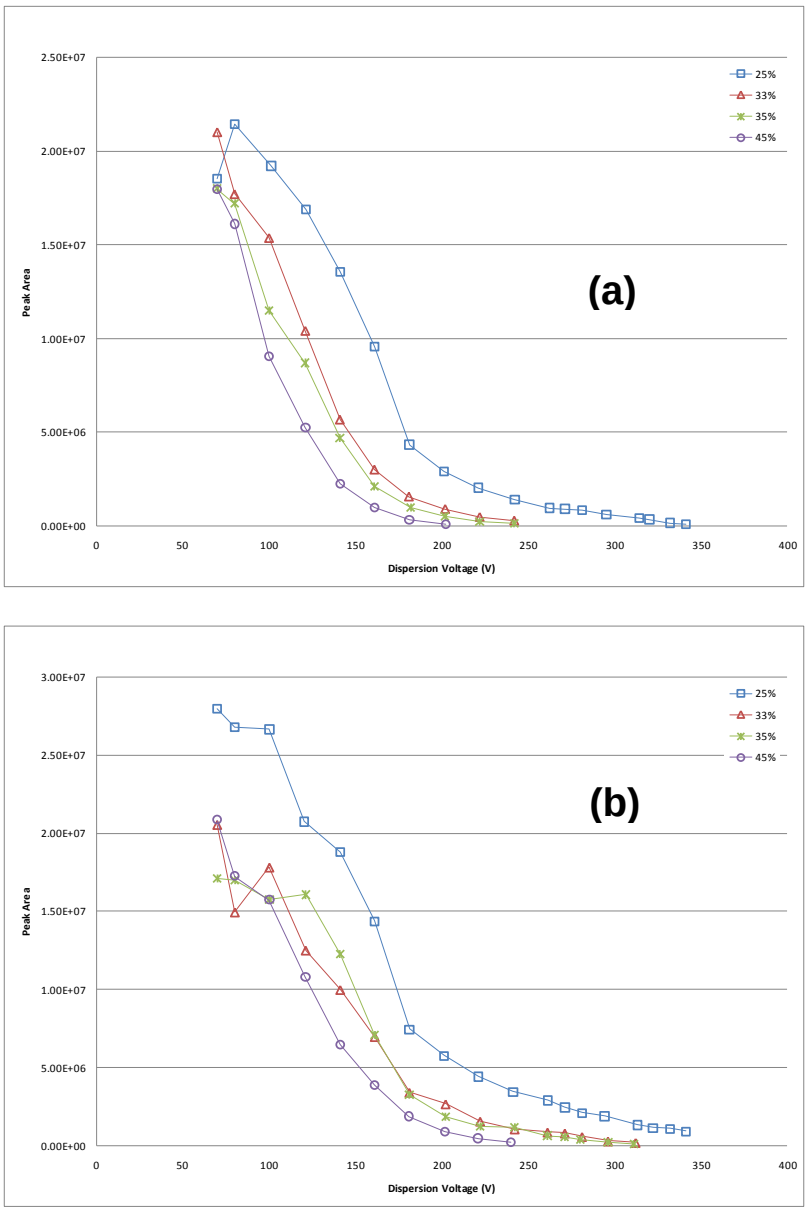

Figure 3-12. Graphs displaying the effect of duty cycle on peak area. Frequency is fixed to 250 kHz **(a)** and 333 kHz **(b)**.

Table 3-1. Summary of the CV, PWHM, R_p, and signal intensity for concentrations from 10 ppm down to 100 ppb.

Concentration	CV (V)	PWHM (V)	R_p	Signal Intensity
10ppm	0.16	0.6	0.26	3.3E+06
1ppm	0.16	0.6	0.25	3.3E+05
500ppb	0.19	0.6	0.30	1.5E+05
250ppb	0.17	0.6	0.29	6.5E+04
100ppb	0.12	0.6	0.19	3.2E+04

CHAPTER 4
CONCLUSIONS

This dissertation presents high-field asymmetric waveform ion mobility spectrometry, or FAIMS, combined with mass spectrometry (FAIMS/MS) as a viable technique for the separation of gas-phase explosive ions at atmospheric pressure. FAIMS can behave as an ion filter that is capable of transmitting only selected compounds in a mixture to pass through to the mass spectrometer. Gaining a better understanding of how this technique separates explosive ions can lead to improved explosive detection. The application of FAIMS/MS to explosive analysis can improve signal-to-noise, while reducing analysis time. The main purpose of this dissertation was to investigate the applicability of novel cell geometries and waveform approaches for FAIMS as a separation tool to be utilized in combination with an atmospheric pressure chemical ionization/mass spectrometry (APCI/MS) system.

The three different geometries of FAIMS cells studied and were cylindrical, hemispherical, and spherical. FAIMS experiments were conducted on the molecular ions of several explosives to determine how their signal intensity, resolution and resolving power were affected in relation to the geometry. The highest sensitivity was obtained by the spherical FAIMS electrode with every explosive that was attempted. Additionally, the spherical FAIMS electrode allowed better resolving power and resolution values than either cylindrical cell. The increased transmission allows the utilization of larger electrode radii, which will help to increase resolution. Hemispherical FAIMS was also shown to improve sensitivity, resolution, and resolving power when compared to the cylindrical cell. It was found that the hemispherical electrodes allow for better resolution when compared to the spherical electrodes. The need of these novel

electrode geometries would be dependent on what the analyst needs, whether it be more resolution with increased but adequate sensitivity (hemispherical), or increased sensitivity with adequate resolution (spherical). The analytical performance of spherical FAIMS/MS was evaluated for TNT to provide information on its quantitative capability. The best CV repeatability was obtained at higher dispersion voltages (-2000 to -3378 V). Two MS scan modes, full-scan and SIM, were tested for LOD and LDR. The method provided limits of detection for TNT down to 4 ppb for full1scan and 1 ppb for SIM. Although full-scan MS provided higher LOD and LDR values, it is still a vital explosive analysis mode because it provides more information about the ion.

The implementation of square wave FAIMS on a miniature planar system was also demonstrated. The ability to independently control frequency, amplitude, and duty cycle of a square waveform can aid in a more complete characterization of FAIMS in terms of transmission, resolution, and separation in comparison to a sum of sines waveform was shown. Square wave FAIMS was displayed to provide better separation and resolving power within the available voltage range and this behavior was verified at higher voltages with the SIMION modeling program. The increase of frequency was shown to increase sensitivity as well as peak area, but had no effect on compensation voltage or resolving power. Experiments showed that the lower the duty cycle the higher the signal intensity. Duty cycle decreases also showed a 30-35% improvement in compensation voltage and resolving power. Comparison of experiments with the sum of sines waveform shows that a square wave technology would be ideal in terms of separation and resolving power.

Future Work

Curved FAIMS Cells

There are many opportunities for future work in this project. The variation of the analytical gap and dispersion voltage would affect the ion transmission and resolution in curved geometry FAIMS cells. Gap size is related to transmission efficiency and resolution. For example, ions with higher mobility values will come closer to the electrodes because of their larger ion amplitude oscillation in the high portion of the asymmetric waveform. These ions will have a better chance of being lost to the electrodes, which will reduce the transmission efficiency through the analyzer region. Since the non-uniformity of the electric field in a curved electrode is aiding the focusing of the ions, it will be advantageous to explore if gap size is a dominant factor in transmission loss or is an insignificant factor when compared to the strong focusing properties in the cell. In other words, it would be beneficial to evaluate whether or not reducing the gap size in a curved geometry will have a negative effect on transmission as it does in a planar cell.

Higher dispersion voltages are needed in order to improve transmission. Further studies can evaluate explosive ion transmission and separation at higher dispersion voltages on curved geometries. Efforts should also continue to explore other geometries in order to characterize all advantages/disadvantages of these novel electrodes. Further studies are also required to improve the sensitivity to be able to use FAIMS as a quantitative method. Finally, computer simulations of various electrode radius sizes and geometries should also be performed in order to compare transmission and resolution.

FAIMS Waveforms

It would be advantageous to improve our understanding of how ions behave under the influence of different parameters of FAIMS, such as different waveforms, in order to apply the optimum condition when more sensitivity or resolution is required for the application of interest. Further studies should be performed to compare square and sine waveforms with different explosives and mixture of explosives as a function of cell dimensions with different cell geometries. Additional experiments using FAIMS waveforms could include the evaluation of other waveform types, higher frequencies, and duty cycles. Finally, computer simulations of various waveform types should be performed to explore the viability of these waveforms.

LIST OF REFERENCES

1. Moore, D. S., *Review of Scientific Instruments* **2004,** *75* (8), 2499-2512.

2. Yinon, J., *Journal of Chromatography A* **1996,** *742* (1-2), 205-209.

3. Sigman, M. E.; Clark, C. D.; Fidler, R.; Geiger, C. L.; Clausen, C. A., *Rapid Commun. Mass Spectrom.* **2006,** *20* (19), 2851-2857.

4. Sigman, M. E.; Ma, C. Y., *Journal of Forensic Sciences* **2001,** *46* (1), 6-11.

5. Pan, X. P.; Zhang, B. H.; Tian, K.; Jones, L. E.; Liu, J.; Anderson, T. A.; Wang, J. S.; Cobb, G. P., *Rapid Commun. Mass Spectrom.* **2006,** *20* (14), 2222-2226.

6. Mathis, J. A.; McCord, B. R., *Rapid Commun. Mass Spectrom.* **2005,** *19* (2), 99-104.

7. Yinon, J.; Zitrin, S., *The Analysis of Explosives*. Pergamon Press: New York, NY, 1981; Vol. 4.

8. Beveridge, A., *Forensic Investigations of Explosives*. Taylor & Francis Ltd.: Bristol, PA, 1998.

9. Na, N.; Zhang, C.; Zhao, M. X.; Zhang, S. C.; Yang, C. D.; Fang, X.; Zhang, X. R., *Journal of Mass Spectrometry* **2007,** *42* (8), 1079-1085.

10. Gapeev, A.; Yinon, J., *Journal of Forensic Sciences* **2004,** *49* (2), 227-237.

11. Fu, X. F.; Zhang, Y.; Shi, S. H.; Gao, F.; Wen, D. W.; Li, W.; Liao, Y. P.; Liu, H. W., *Rapid Commun. Mass Spectrom.* **2006,** *20* (19), 2906-2914.

12. Tachon, R.; Pichon, V.; Le Borgne, M. B.; Minet, J. J., *Journal of Chromatography A* **2007,** *1154* (1-2), 174-181.

13. Buryakov, I. A., *Journal of Chromatography B-Analytical Technologies in the Biomedical and Life Sciences* **2004,** *800* (1-2), 75-82.

14. Purves, R. W.; Guevremont, R.; Day, S.; Pipich, C. W.; Matyjaszczyk, M., *Review of Scientific Instruments* **1998,** *69*, 4094-4105.

15. Eiceman, G. A.; Tadjikov, B.; Krylov, E.; Nazarov, E. G.; Miller, R. A.; Westbrook, J.; Funk, P., *Journal of Chromatography A* **2001,** *917* (1-2), 205-217.

16. Eiceman, G. A.; Nazarov, E. G.; Miller, R. A.; Krylov, E. V.; Zapata, A. M., *Analyst (Cambridge, United Kingdom)* **2002,** *127* (4), 466-471.

17. Barnett, D. A.; Purves, R. W.; Ells, B.; Guevremont, R., *Journal of Mass Spectrometry* **2000,** *35*, 976-980.

18. Robinson, E. W.; Sellon, R. E.; Williams, E. R., *International Journal of Mass Spectrometry* **2007,** *259* (1-3), 87-95.

19. Tang, K. Q.; Li, F. M.; Shvartsburg, A. A.; Strittmatter, E. F.; Smith, R. D., *Analytical Chemistry* **2005,** *77* (19), 6381-6388.

20. Buryakov, I. A.; Krylov, E. V.; Nazarov, E. G.; Rasulev, E. K., *International Journal of Mass Spectrometry and Ion Processes* **1993,** *128*, 143-148.

21. Guevremont, R.; Purves, R. W., *Review of Scientific Instruments* **1999,** *70*, 1370-1383.

22. Krylov, E. V., *Technical Physics* **1999,** *44*, 113-116.

23. Guevremont, R.; Purves, R. W.; Barnett, D. A.; Ding, L. Y., *International Journal of Mass Spectrometry* **1999,** *193* (1), 45-56.

24. Buryakov, I. A.; Kolomiets, Y. N.; Luppu, B. V., *Journal of Analytical Chemistry* **2001,** *56* (4), 336-340.

25. Buryakov, I. A., *Talanta* **2003,** *61* (3), 369-375.

26. Eiceman, G. A.; Karpas, Z., *Ion Mobility Spectrometry*. 2nd ed; CRC Press: Boca Raton, FL, 2005.

27. Barnett, D. A.; Ells, B.; Guevremont, R.; Purves, R. W., *Journal of the American Society for Mass Spectrometry* **1999,** *10*, 1279-1284.

28. Karasek, F. W., *Research-Development* **1970,** *21* (3), 34-37.

29. Cohen, M. J.; Karasek, F. W., *Journal of Chromatographic Science* **1970,** *8* (6), 330-337.

30. Karasek, F. W.; Kilpatri.Wd; Cohen, M. J., *Analytical Chemistry* **1971,** *43* (11), 1441-1447.

31. Zimmermann, S.; Barth, S.; Baether, W. K. M.; Ringer, J., *Analytical Chemistry* **2008,** *80* (17), 6671-6676.

32. Ewing, R. G.; Atkinson, D. A.; Eiceman, G. A.; Ewing, G. J., *Talanta* **2001,** *54* (3), 515-529.

33. Lu, Y.; O'Donnell, R. M.; Harrington, P. B., *Forensic Science International* **2009,** *189* (1-3), 54-59.

34. Kemper, P. R.; Dupuis, N. F.; Bowers, M. T., *International Journal of Mass Spectrometry* **2009,** *287* (1-3), 46-57.

35. Tao, L.; Dahl, D. B.; Perez, L. M.; Russell, D. H., *J Am Soc Mass Spectrom* **2009,** *20* (9), 1593-1602.

36. Creaser, C. S.; Griffiths, J. R.; Bramwell, C. J.; Noreen, S.; Hill, C. A.; Thomas, C. L. P., *Analyst,* **2004,** *129* (11), 984-994.

37. Revercomb, H. E.; Mason, E. A., *Analytical Chemistry* **1975,** *47* (7), 970-983.

38. Dugourd, P.; Hudgins, R. R.; Clemmer, D. E.; Jarrold, M. F., *Review of Scientific Instruments* **1997,** *68*, 1122-1130.

39. Kanu, A. B.; Haigh, P. E.; Hill, H. H., *Analytica Chimica Acta* **2005,** *553* (1-2), 148-159.

40. Guevremont, R., *Journal of Chromatography A* **2004,** *1058* (1-2), 3-19.

41. Viehland, L. A.; Guevremont, R.; Purves, R. W.; Barnett, D. A., *International Journal of Mass Spectrometry* **2000,** *197*, 123-130.

42. Shvartsburg, A. A.; Tang, K. Q.; Smith, R. D., *Journal of the American Society for Mass Spectrometry* **2004,** *15* (10), 1487-1498.

43. Purves, R. W.; Guevremont, R., *Analytical Chemistry* **1999,** *71* (13), 2346-2357.

44. Barnett, D. A.; Ells, B.; Guevremont, R., *Journal of the American Society for Mass Spectrometry* **2000,** *11* (12), 1125-1133.

45. Ouyang, Z.; Noll, R. J.; Cooks, R. G., *Analytical Chemistry* **2009,** *81* (7), 2421-2425.

46. Paul, W.; Steinwedel, H. U.S. Patent; Apparatus for Separating Charged Particles of Different Specific Charges. 1960; Vol. 2939952.

47. Watson, J. T., Types of Mass Spectrometers. In *Introduction to Mass Spectrometry*, 3rd ed.; Lippincott-Raven Publishers: Philadelphia, PA, 1997; p 80.

48. Finnigan LCQ Hardware Manual Classic Series, 97000-97053 Revision B ed.; San Jose, CA, 2003; pp 2-17 - 2-24.

49. Wuerker, R. F.; Shelton, H.; Langmuir, R. V., *Journal of Applied Physics* **1959,** *30* (3), 342-349.

50. March, R. E., *Journal of Mass Spectrometry* **1997,** *32* (4), 351-369.

51. Carnahan, B. L.; Tarassov, A. S. Ion mobility spectrometer, 1995.

52. Guevremont, R.; Purves, R.; Barnett, D. Spherical side-to-side FAIMS. 359644 & 226965, February 7, 2003.

53. Guevremont, R.; Purves, R. W. FAIMS Apparatus and Method with Ion Diverting Device. 6825461, November 30, 2004.

54. Guevremont, R.; Ding, L. Y.; Ells, B.; Barnett, D. A.; Purves, R. W., *Journal of the American Society for Mass Spectrometry* **2001,** *12* (12), 1320-1330.

55. Hoffman, E. D.; Stroobant, V., *Mass Spectrometry Principles and Applications*. 2nd ed.; John Wiley and Sons: West Sussex, England, 2002.

56. Spangler, G. E.; Lawless, P. A., *Analytical Chemistry* **1978,** *50* (7), 884-892.

57. Spangler, G. E.; Lawless, P. A., *Analytical Chemistry* **1978,** *50* (2), 290-294.

58. Long, G. L.; Winefordner, J. D., *Analytical Chemistry* **1983,** *55* (7), A712-&.

59. Guevremont, R., FAIMS. www.faims.com, September 23, 2009.

60. Barnett, D. A.; Belford, M.; Dunyach, J. J.; Purves, R. W., *Journal of the American Society for Mass Spectrometry* **2007,** *18*, 1653-1663.

61. Purves, R. W.; Guevremont, R.; Day, S.; Pipich, C. W.; Matyjaszczyk, M. S., *Review of Scientific Instruments* **1998,** *69* (12), 4094-4105.

62. Krylov, E.; Nazarov, E. G., *International Journal of Mass Spectrometry* **2009,** *285*, 149-156.

63. Papanastasiou, D.; Wollnik, H.; Rico, G.; Tadjimukhamedov, F.; Mueller, W.; Eiceman, G. A., *Journal of Physical Chemistry A* **2008,** *112* (16), 3638-3645.

64. Krylov, E. V., *Instruments and Experimental Techniques* **1997,** *40* (5), 628-631.

65. Shvartsburg, A. A.; Tang, K.; Smith, R. D., *Journal of the American Society for Mass Spectrometry* **2005,** *16* (1), 2-12.

66. Krylov, E. V.; Nazarov, E. G.; Miller, R. A., *International Journal of Mass Spectrometry* **2007,** *266*, 76-85.

67. Shvartsburg, A. A.; Smith, R. D., *Journal of the American Society for Mass Spectrometry* **2008,** *19* (9), 1286-1295.

68. Manura, D. J.; Dahl, D., *SIMION Version 8.0 User Manual*. 2007.

69. Eiceman, G. A.; Krylov, E.; Krylova, N.; Nazarov, E. G.; Miller, R. A., *Analytical Chemistry* **2004,** *76*, 4937-4944.

70. Matz, L. M.; Tornatore, P. S.; Hill, H. H., *Talanta* **2001,** *54* (1), 171-179.

71. Tam, M.; Hill, H. H., *Analytical Chemistry* **2004,** *76* (10), 2741-2747.

72. Rorrer III, L. C.; Yost, R. A., *International Journal of Mass Spectrometry* **2010,** (In Press).

73. Krylov, E. V., *International Journal of Mass Spectrometry* **2003,** *225*, 39-51.

74. Rokushika, S.; Hatano, H.; Baim, M. A.; Hill, H. H., *Analytical Chemistry* **1985,** *57* (9), 1902-1907.

75. Shvartsburg, A. A.; Smith, R. D., *Journal of the American Society for Mass Spectrometry* **2007,** *18*, 1672-1681.

BIOGRAPHICAL SKETCH

Marilyn Prieto was born in 1977, in Rio Piedras, Puerto Rico. She attended Florida International University where she received a Bachelor of Science degree in chemistry in 2005 along with a forensic science certification. Her undergraduate research involved the development of a universal GC/MS/MS method for the detection of ignitable liquid residues (ILR) under the advisement of Dr. Jose R. Almirall. After graduating, she traveled to Midland, Michigan for an internship in Dow Corning Corporation where her research dealt with making emulsions that consisted of smaller particle sizes from novel anionic surfactants.

After completing the internship, she travelled to Gainesville, Florida in 2006 to commence her graduate career in analytical chemistry under the supervision of Dr. Richard A. Yost. Her graduate interests have been mostly focused on the basic development and characterization of a portable explosives detection instrument which utilizes and maximizes the technology of High-Field Asymmetric Waveform Ion Mobility Spectrometry/Mass Spectrometry (FAIMS/MS). She completed her graduate career and received her PhD degree in August 2010.